Mapping the Spectrum of Light Quark Mesons and Gluonic Excitations with Linearly Polarized Photons

Presentation to PAC30 – The GlueX Collaboration
(Dated: July 6, 2006)

The goal of the GlueX experiment is to provide critical data needed to address one of the outstanding and fundamental challenges in physics – the quantitative understanding of the confinement of quarks and gluons in quantum chromodynamics (QCD). Confinement is a unique property of QCD and understanding confinement requires an understanding of the soft gluonic field responsible for binding quarks in hadrons. Hybrid mesons, and in particular exotic hybrid mesons, provide the ideal laboratory for testing QCD in the confinement regime since these mesons explicitly manifest the gluonic degrees of freedom. Photoproduction is expected to be particularly effective in producing exotic hybrids but there is little data on the photoproduction of light mesons. GlueX will use the coherent bremsstrahlung technique to produce a linearly polarized photon beam. A solenoid-based hermetic detector will be used to collect data on meson production and decays with statistics after the first year of running that will exceed the current photoproduction data in hand by several orders of magnitude. These data will also be used to study the spectrum of conventional mesons, including the poorly understood excited vector mesons. In order to reach the ideal photon energy of 9 GeV for this mapping of the exotic spectrum, 12 GeV electrons are required. This document describes the physics goals, the beam and apparatus, and plans for the first two years of commissioning and data-taking.

I. OVERVIEW

A. QCD and Light Meson Spectroscopy

The observation, nearly four decades ago, that mesons are grouped in nonets, each characterized by unique values of J^{PC} – spin (J), parity (P) and charge conjugation (C) quantum numbers – led to the development of the quark model. Within this picture, mesons are bound states of a quark (q) and antiquark ($\bar{q}$). The three light-quark flavors (*up*, *down* and *strange*) suffice to explain the spectroscopy of most – but not all – of the lighter-mass mesons (below 3 GeV/c^2) that do not explicitly carry heavy flavors (charm or beauty). Early observations yielded only those J^{PC} quantum numbers consistent with a fermion-antifermion bound state. The J^{PC} quantum numbers of a $q\bar{q}$ system with total quark spin, $\vec{S}$, and relative angular momentum, $\vec{L}$, are determined as follows: $\vec{J} = \vec{L} + \vec{S}$, $P = (-1)^{L+1}$ and $C = (-1)^{L+S}$. Thus J^{PC} quantum numbers such as 0^{--}, 0^{+-}, 1^{-+} and 2^{+-} are not allowed and are called *exotic* in this context.

Our understanding of how quarks form mesons has evolved within quantum chromodynamics (QCD) and we now expect a richer spectrum of mesons that takes into account not only the quark degrees of freedom but also the gluonic degrees of freedom. Gluonic mesons with no quarks (*glueballs*) are expected. These are bound states of pure glue and since the quantum numbers of low-lying glueballs (below 4 GeV/c^2) are not exotic, they should manifest themselves as extraneous states that cannot be accommodated within $q\bar{q}$ nonets. But their unambiguous identification is complicated by the fact that they can mix with $q\bar{q}$. Excitations of the gluonic field binding the quarks can also give rise to so-called *hybrid* mesons that can be viewed as bound states of a quark, antiquark and valence gluon ($q\bar{q}g$). An alternative picture of hybrid mesons, one supported by lattice QCD [1], is one in which a gluonic flux tube forms between the quark and antiquark and the excitations of this flux tube lead to so-called *hybrid* mesons. Actually the idea of flux tubes, or strings connecting the quarks, originated in the early 1970's [2] to explain the observed linear dependence of the mass-squared of hadrons on spin (Regge trajectories). Conventional $q\bar{q}$ mesons arise when the flux tube is in its ground state. Hybrid mesons arise when the flux tube is excited and some hybrid mesons can have a unique signature, exotic J^{PC}, and the spectroscopy of these exotic hybrid mesons is simplified because they do not mix with conventional $q\bar{q}$ states.

The level splitting between the ground state flux tube and the first excited transverse modes is π/r, where r is the separation between the quarks, so the hybrid spectrum should lie about 1 GeV/c^2 above the ground state spectrum. While the flux-tube model [3] has all hybrid nonets degenerate in mass, from lattice gauge calculations [4], one expects the lightest $J^{PC} = 1^{-+}$ exotic hybrid to have a mass of about 1.9 GeV/c^2. In this discussion the motion of the quarks was ignored, but we know from general principles [3] that an approximation that ignores the impact of the flux tube excitation and quark motion on each other seems to work quite well. It should be noted, also, the in the large-N_c limit of QCD, exotic hybrids are expected to have narrow widths, comparable to $q\bar{q}$ states [5].

In the coming years there will be significant computational resources [6] dedicated to understanding non-perturbative QCD including confinement using lattice techniques. The prediction of the hybrid spectrum, including decays, will be a key part of this program but experimental data will be needed to verify these calculations. The spectroscopy of exotic mesons provides a clean and attractive starting point for the study of glu-

onic excitations.

The GlueX experiment is designed to collect data of unprecedented statistics and quality surpassing existing data on the photoproduction of light mesons by several orders of magnitude after the first year of data-taking. As part of the program of identifying exotic hybrid mesons, these data will also be used to understand the conventional meson spectrum including the poorly understood excited vector mesons.

The physics of GlueX has been presented to an external review committee, several town meetings of the nuclear physics community leading up to the Nuclear Science Advisory Committee (NSAC) Long Range Plan, to three JLAB Program Advisory Committees and most recently to the Department of Energy (DOE) Office of Nuclear Physics Science Review of the Proposed 12 GeV Upgrade in April 2005.

B. Using Linearly Polarized Photons

As will be discussed below, there are tantalizing suggestions, mainly from experiments using beams of π mesons, that exotic hybrid mesons exist. The evidence is by no means clear cut, owing in part, to the apparently small production rates for these states in the decay channels examined. It is safe to conclude that the extensive data collected to date with π probes have not uncovered the hybrid meson spectrum. Models, like the flux-tube model, however, indicate the photon is a probe that should be particularly effective in producing exotic hybrids, but data on photoproduction of light mesons are sparse indeed.

The first excited transverse modes of the flux tube are degenerate and correspond to clockwise or counterclockwise rotations of the flux tube about the axis joining the quark and antiquark fixed in space with $J = 1$ [3]. Linear combinations of these two modes are eigenstates of parity and lead to $J^{PC} = 1^{+-}$ and $J^{PC} = 1^{-+}$ for the excited flux tube. When these quantum numbers are combined with those of the $q\bar{q}$ with $\vec{L} = 0$ and $\vec{S} = 1$ (quark spins aligned) three of the six possible J^{PC} have exotic combinations: 0^{+-}, 1^{-+} and 2^{+-}. A photon probe is a virtual $q\bar{q}$ with quark spins aligned. In contrast when the $q\bar{q}$ have $\vec{L} = 0$ and $\vec{S} = 0$ (spins anti-aligned), the resulting quantum numbers of the hybrid meson are not exotic. Pion probes are $q\bar{q}$ with quark spins anti-aligned. If we view one outcome of the scattering process as exciting the flux tube binding the quarks in the probe, the suppression of exotic hybrids in π-induced reactions is not surprising – a spin flip of one of the quarks is required followed by the excitation of the flux tube. In contrast the spins of the virtual quarks in the photon probe are properly aligned to lead to exotic hybrids. Phenomenological studies quantitatively support this picture predicting that the photoproduction cross-sections for exotic mesons are comparable to those for conventional mesons [7, 8].

The quantum numbers of mesons produced in the GlueX experiment will require an amplitude analysis based on measuring the energy and momentum of their decay products. Linear polarization of the incident photon is required for a precision amplitude analysis to identify exotic quantum numbers, to understand details of the production mechanism of exotic and conventional mesons and to remove backgrounds due to conventional processes. Linear polarization will be achieved using the coherent bremsstrahlung technique. Details of how polarization information is used and how polarization is achieved will be given below.

We will show below, that for a solenoid-based detector system, and given the required mass reach required for mapping the spectrum of exotic hybrid mesons, a photon energy of ≈ 9 GeV is ideal. To achieve the requisite degree of linear polarization for 9 GeV photons using coherent bremsstrahlung requires a minimum electron energy of 12 GeV.

C. Detector & Beam Overview

A schematic of the GlueX detector and beamline is shown in Figure 1. Note that the drawing is not to scale. To carry out the amplitude analysis that will identify exotic hybrid mesons, the beam must have sufficient energy and be linearly polarized and the detector must be hermetic and have excellent resolution. We now discuss these features of the GlueX beam and detector.

1. Photon Beam

The photon beam is produced by having a low-emittance 12 GeV electron beam incident on a thin (≈ 20 μm) diamond wafer. After passing through the wafer, the electron beam is bent by a dipole magnet (the *tagger* magnet) into the beam dump. A small fraction, about 0.01% of the electrons, emit a photon via incoherent bremsstrahlung or coherent bremsstrahlung, the latter leading to an enhancement over the incoherent spectrum at a photon energy determined by the angle between the incident electron direction and the wafer. By exploiting the tight energy–angle correlation for the coherent photons, collimation of the photon beam can be used to enhance the fraction of photons of the coherent radiation incident on the GlueX target. This has the effect of increasing the degree of linear polarization and eliminating a large fraction of the low-energy photons that dominate the incoherent component of the spectrum. An active collimator, with a 3.5 mm hole, will be placed just upstream of the GlueX detector and about 75 m downstream of the tagger magnet. The electrons emitting 8.5 to 9.0 GeV bremsstrahlung photons will be momentum analyzed using a focal plane spectrometer leading to a photon energy resolution of 0.2%. At the start of operations, the rate of tagged photons incident on the GlueX detector will be 10^7/s. During the first two

years of operation, the plan is to steadily increase this up to the ultimate maximum rate of 10^8/s. A linearly polarized photon beam using coherent bremsstrahlung has been used in HALL B. A review of the GLUEX photon beam line and tagger magnet was successfully completed in January 2006.

2. Superconducting Solenoid

The GLUEX design is based on a solenoidal magnet – the magnetic field confining electromagnetic backgrounds, in the form of e^+e^- pairs, in tight spiral orbits within a beam pipe. Such a design is superior to a spectrometer based on a dipole design that would deflect electrons and positrons in opposite directions producing a plane of charged particle backgrounds that would require deadening regions of detectors in this plane, thus degrading the hermeticity required by the amplitude analysis.

The superconducting solenoid to be used in the GLUEX detector was built over 30 years ago for the LASS experiment at SLAC [9]. The magnet has an inside clear bore diameter of 185 cm and an overall clear bore length of 495 cm. The maximum central field is 2.24 T with a field that is uniform to within ±3% within the clear bore and to within ±1% along the central axis within the clear bore. The LASS experiment studied mesons produced with an 11 GeV/c K^- beam and the design of GLUEX represents, to some extent, an upgrade to the LASS design. In 1985 the solenoid was dismantled and moved to LAMPF at Los Alamos for use in the MEGA experiment. Only three of the four coils were used in that setup. In 2000, a team, including two of the original designers and builders of the magnet, reviewed the state of the magnet and concluded that the costs associated with moving and refurbishing the magnet for use in GLUEX were warranted. In 2002 the magnet was disassembled and moved to the Indiana University Cyclotron Facility (IUCF) where, to date, all four coils have been tested and three have been repaired. The state of coil testing and repairs was reviewed in November 2004 by an external committee.

3. Detector Subsystems

Inside the clear bore of the magnet a 30 cm-long liquid hydrogen target is surrounded by scintillation counters (START), a cylindrical drift chamber array (CDC) and an electromagnetic lead/scintillating fiber calorimeter with a barrel geometry (BCAL). Upstream of the target is a lead/scintillator electromagnetic calorimeter to be used as an offline veto (UPV) and downstream of the target are an array of planar drift chambers (FDC). Outside and downstream of the clear bore of the magnet are a Čerenkov counter, a wall of scintillation counters (TOF) to measure time-of-flight and an electromagnetic calorimeter (FCAL) consisting of a stack of lead-glass blocks.

The overall physics and detector design was first reviewed by an external committee in December 1999. Another external committee reviewed the GLUEX detector in October 2004. R&D projects for subsystems, including tests at the Serpukhov and TRIUMF accelerators, have been carried out over the last five years. Beam tests for BCAL will take place in HALL B starting in Fall, 2006. Beam tests for FCAL and tracking chambers will be carried out in HALL B in 2007.

4. Readout and Data Rates

The GLUEX experiment is designed to record data at a rate of 15 kHz. For the initial photon flux of 10^7/s, the level 1 trigger will result in a 15 kHz rate of recorded events of which about 1.5 kHz will be interesting physics. At 10^8/s the level 1 rate will be 200 kHz and a level 3 software trigger will be required to reduce this to 15 kHz. To meet the requirement of a system with zero dead-time, a pipelined approach is required. The digitized information will be stored for several μs while the level 1 trigger is formed. Multiple events must be buffered within the digitizer modules and read out while the front ends continue to acquire new events.

Two basic types of readout electronics will be used in GLUEX, FADCs (flash ADCs) and TDCs. Detectors which measure energy will be continuously sampled with FADCs while detectors which require precise time measurements will use a multi-hit TDC. The photon tagger, START counter, FDC anodes, Čerenkov counter, BCAL and TOF detectors will be read out by multi-hit TDCs. A high resolution pipeline TDC module has been developed for use at JLAB [10]. The calorimeters, Čerenkov counter and TOF will be read out with 10-bit, 250 MHz FADCs. The CDC and FDC chambers will be read out with a slower (≈100 MHz) 10 or 12 bit FADC. The exact read out electronics requirements for these detectors is the subject of ongoing R&D efforts. Given the 15 kHz rate for recording data, the GLUEX experiment will produce data at rate of 1 petabyte each year.

An external review committee reviewed the electronics in July 2003 and in each of the last three years a workshop was held devoted to GLUEX electronics issues.

5. Analysis Issues

Amplitude analysis has typically been both statistics and computationally limited. The fitting procedure is numerically intense, both in terms of evaluating amplitudes and in terms of memory usage on the computational nodes. In addition, careful systematic studies of the robustness of results need to be done. These are made more difficult as the statistics of data samples increase. Historically, experimentalists have carried out

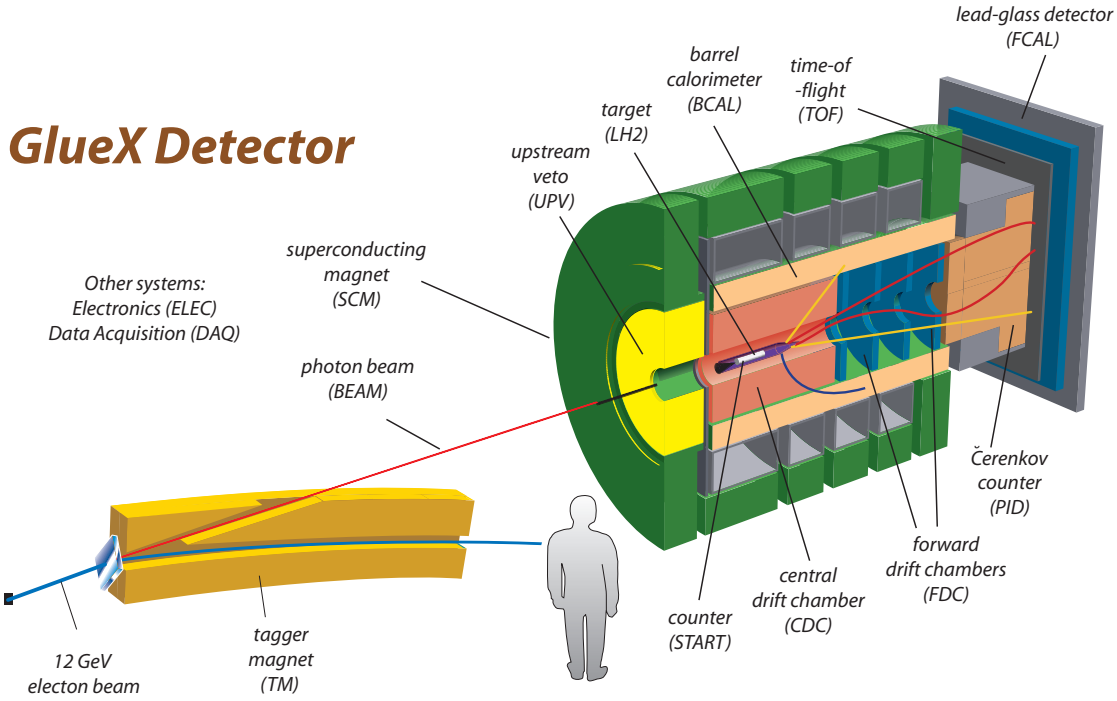

FIG. 1: A schematic of the GlueX detector and beam (not to scale). Please see Table III for institutional responsibilities for GlueX detector subsystems.

amplitude analysis and published results such as intensities and phases. These results were then used by theorists in comparing to predictions. Because of the close association between theorists and experimentalists in GlueX, one goal of GlueX is to get input from theorists at a much earlier stage in the analysis. This is best accomplished by building analysis tools for which it is easy to change physics amplitude generators. In particular, such a switch should not require new Monte Carlo data and should make it possible to test predictions directly with the data. To address these issues, members of the GlueX collaboration are both involved in ongoing amplitude analysis of existing data sets as well as building tool sets which can evolve to handle the needs of GlueX.

The Indiana University (IU) group has continued to analyze pion induced reactions using data from the Brookhaven E852 experiment. Some of these results will be discussed below. The key features that are relevant here are the work done to analyze more than one isospin channel for related final states at the same time, *e.g.*, $\pi^- p \to \pi^-\pi^-\pi^+ p$ and $\pi^- p \to \pi^-\pi^0\pi^0 p$. In addition a great deal of work went into optimizing the fitting procedure for parallel processing.

The Carnegie Mellon (CMU) group is in the process of analyzing CLAS photo-production data to look for baryon resonances. While the first results are just starting to come out, several man years of effort went into developing a general purpose set of tools that in principle could be used in other experimental contexts. These can be broadly broken into several pieces. At CLAS photon energies, both s and t-channel processes contribute and the typical generators based on E852 analysis do not handle such mixed terms. The CMU group implemented an amplitude package based on covariant tensor formalism [11–15]. This formalism was developed in a more general context than the standard helicity formalism, and therefore avoids most of the pitfalls with that formalism. This physics generator that can be easily changed, either adding additional amplitudes, form-factors or even the underlying physics without changing any data or Monte Carlo data sets. The second piece is a fitting tool that is optimized for speed and has the ability to handle multiple data sets from potentially different experiments simultaneously. These tools include flexibility in defining the amplitude rules, the ability to switch between different minimization algorithms (MINUIT, FUMILI) as a fit proceeds, and a set of tools to systematically vary the data sets that go into the fits. This analysis framework is easy to use and is designed to avoid the typical pitfalls that are common when managing many files. Finally, development has started on a set of tools to visualize results and compute and display typical observables such as cross sections. The results are stored in a searchable database that is keyed by fit parameters and allows easy comparison of related fits. In CLAS, these tools are being used to analyze photoproduction reactions on the proton leading to ηp, $\eta' p$, ωp, $\pi^+\pi^- p$, $K^+\Lambda$, and $\pi^0 p$ and $\pi^+ n$, both individually and coupled together.

It is anticipated that desirable features from both the IU and CMU work will evolve into a general analysis package that will be able to handle the large data sets coming out of GlueX as well as allowing the experiment

to take full advantage of the input of the theory group.

The GLUEX collaboration has held several workshops devoted to some combination of analysis and computational issues in September 2000, June 2002, May 2003, February 2005 and February 2006. These workshops have included physicists and computer scientists from other experiments.

D. Summary

This concludes the overview of the physics goals of GLUEX, how those goals will be realized and the activities of the collaboration over the last six years. More detailed information can be found in the Design Reports and the reports of the various review committees. These documents have been collected for PAC30 members on the GLUEX website: `www.gluex.org`.

II. PHYSICS OF GLUONIC EXCITATIONS

A. Lattice QCD

The run-up to the GLUEX experiment occurs at a time of great progress for Lattice QCD calculations. Recent improvements in numerical algorithms make large scale phenomenological studies with dynamical ("unquenched") lattices practical. In addition, through programs like SciDAC the nuclear theory community has at its command a much greater volume of computing resources which can be brought to bear on the physics relevant to the GLUEX experiment.

1. *Light-quark meson mass spectrum*

Examples of different aspects of the state of the art in conventional meson spectrum studies are the recent works by the collaborations MILC[16] and BRG[17]. The MILC study utilizes a set of fully dynamical, $N_F = 2_{u,d}+1_s$, gauge configurations with relatively small pion masses ($m_\pi \sim 300$ MeV) and with rather fine lattice spacings ($a \sim 0.09$ fm). Their choice of simple point-like fermion bilinear interpolating fields for mesons limits their spectrum to non-exotic quantum numbers with $J \leq 1$. The BRG collaboration work (like the LHPC baryon spectrum study in [18]), while performed within the problematic quenched approximation, takes advantage of the advanced variational analysis technique which, it is demonstrated, allows the extraction of a number of excited states in a given J^{PC} channel.

Due to the lack of extensive and reliable data on hybrids, mesons with exotic quantum numbers have been somewhat under-considered in lattice QCD. A summary of virtually all available simulation results [19–27] for the lightest 1^{-+} state mass appears in Figure 2(a). These studies have typically been performed at relatively heavy pion mass, and have usually used quenched and often coarse and unimproved lattices. Despite these caveats, theoretical predictions point to the existence of such a state. In Figure 2(b) the anticipated multi-meson S-wave state threshold masses are plotted indicating that at heavy quark mass the lightest 1^{-+} state is consistent with being a single particle bound state of QCD.

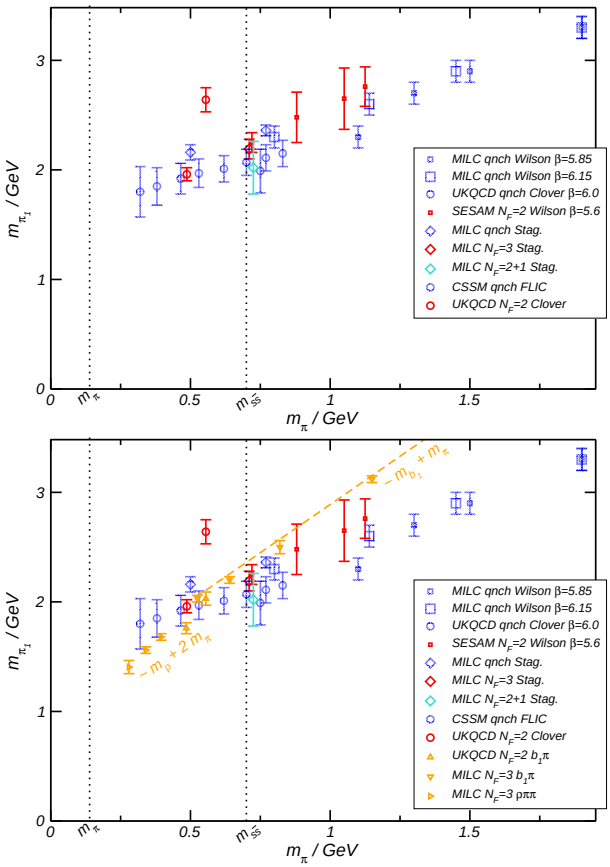

FIG. 2: (a) Summary of lattice results for the mass of lightest 1^{-+} state as a function of the pion mass in the same simulation. (b) Also shown are lattice estimates of the mass of relevant non-interacting S-wave multi-meson thresholds.

It is not a trivial exercise to extrapolate the lattice data shown in Figure 2 to give a value for the mass in the physical limit, but model-based estimates [28] indicate that the mass obtained from dynamical simulations should not show extreme curvature in an extrapolation in m_π^2 to the physical pion mass. Hence it is reasonable to conclude that the lattice data are compatible with a 1^{-+} resonance in the region around 2 GeV, as suggested by various models.

A challenge for future lattice QCD simulations is to investigate the spectrum of the 1^{-+} and other exotic channels in the lighter quark regime where multi-meson states are lightest and where any hybrid meson would appear as an excited state "resonance". Increases in computing resources coupled with application of new theoretical techniques [29] make such analyses possible on the time

scale of the preparations for GlueX. The JLab theory group intends to lead such efforts; by summer 2007 a set of dynamical $N_F = 2+1$ lattices, with pion masses as low as ~ 350 MeV will have been generated that are designed to be ideal for use in spectroscopic calculations. In parallel, good interpolating fields for exotic and conventional quantum numbers up to $J = 3$ are being developed along with the analysis techniques for extracting many excited states. Combining these two ingredients should allow extraction of a considerable fraction of the conventional and exotic spectroscopy in the GlueX energy range. Indeed the anticipation of results from GlueX is a major incentive for the continued study of the exotic and excited meson spectrum in lattice QCD.

2. Photocouplings

The photoproduction of meson resonances at GlueX is likely, in large part, to occur through diagrams where a t-channel meson exchange from the baryon vertex fuses with the incident photon to form the resonance. The amplitude for this diagram is clearly proportional to the electromagnetic transition matrix element between the exchange meson and the resonance. Such matrix elements are amenable to calculation in lattice QCD where previously they have only been considered in models (see next section).

Computing these matrix elements is a major component in the JLab lattice program; already the techniques have been developed and applied to the test-case of conventional radiative transitions in the charmonium system, where the lattice results are found to agree well with both experiment and the successful quark-potential models relevant for heavy-quark systems [30].

Extension of this work to include higher spin mesons and exotics is underway in parallel to the spectrum program and it is anticipated that on a short time scale simulations will be performed at lighter quark masses, making predictions of direct relevance to GlueX.

3. Hadronic decays

Hadronic decays within lattice QCD remain a technical challenge. Naively one can see that this will be so by consideration of the nature of the calculational scheme in which the finite size of the lattice box renders the multi-particle spectrum discrete - removing the possibility of a state decaying into the multi-meson continuum. Nevertheless techniques have been developed to extract decay information, such as the Luscher method which utilizes variation of the size of the lattice box to investigate the phase shift in a two-particle elastic process. A speculative attempt to apply this method to the 1^{-+} channel can be seen in [31] but a considerable extrapolation is required to reach the mass region in which decay can occur. Resources are such that a trial of the Luscher method in a region where such an extrapolation is not required can be expected within the next couple of years.

Another possibility is the method pioneered by Michael and collaborators [27] which artificially tunes parameters (mostly the quark mass) so that a single particle state is nearly degenerate with a two particle state into which in the physical limit it is expected to decay. The Euclidean time dependence of the overlap of the states yields the coupling between them. An extrapolation is then made to the physical limit where the phase-space is non-zero to make a width prediction.

Thus far the decays of a 1^{-+} state into the S-wave channels, πb_1 and[91] πf_1 have been considered - P-wave channels such as $\rho\pi$ appear at higher energy owing to the finite energy cost of applying discrete momentum in a finite box. First results on $N_F = 2$ lattices indicate a partial width for a π_1 at 2 GeV into πb_1 of 400 ± 120 MeV and into πf_1 of 90 ± 60 MeV, where the errors are only statistical. These values are obtained via an extrapolation to the physical point assuming that the coupling is unvarying as the momentum transfer increases, an assumption which is challenged in a model framework in [32] and discussed briefly in the next section.

B. QCD inspired models

Models and empirical intuition are a strong guide to production mechanism expectations at GlueX. For example, the photon with $J^{PC} = 1^{--}$ is expected to scatter from the vacuum (Pomeron exchange) and with momentum transfer in $S, P \ldots$ waves convert into hadrons with $J^{PC} = 1^{--}; 2^{+-}; \ldots$. This potential access to mesons with exotic J^{PC} by Pomeron exchange is unique to photon beams.

In the flux tube model the 2^{+-} state is expected in the same mass range as the 1^{-+} and is formed by the flux-tube containing one unit of intrinsic angular momentum and the $q\bar{q}$ being in spin-triplet. Thus if the photon acts as a hadron with $S_{q\bar{q}} = 1$, any spin-independent excitation of the gluonic degrees of freedom by the (supposedly gluonic) Pomeron will lead rather directly to the 2^{+-} exotic configuration.

For the exotic states with $J^{PC} = 1^{-+}$, predicted in lattice QCD and flux tube models to be among the first excited hybrid states, photoproduction requires non-trivial quantum number exchange. Here again in models $S_{q\bar{q}}(1^{-+}) = 1$, so if the photon is considered to be interacting via its hadronic component, the initial photon spin configuration is a favorable entree to the 1^{-+}.

Historically, Isgur had made qualitative arguments that the photoproduction amplitudes for hybrids made of light quarks will be comparable to those of conventional mesons [33] . This was based on the Cabibbo-Radicati sum rule and duality between the gluonic contributions to the pion charge radius and the photoexcitation of hybrid mesons by electric dipole radiation. Close and Dudek [34, 35] performed the first explicit calculation of these

amplitudes in the flux-tube model, which quantitatively confirmed Isgur's speculation. For light flavors, the $E1$ transition amplitudes to hybrid mesons were found to be comparable to those for conventional mesons. In particular the $\gamma a_2^{\pm} \to \pi_1^{\pm}$ amplitude is expected to contribute to the $\gamma p \to \pi_1^+ n$ via a_2 exchange and is not suppressed.

These calculations also apply to ρ exchange, which via the photon $E1$ multipole can convert to 2^{+-}. This too is not suppressed and so a non-diffractive production of the 2^{+-} may be expected in addition to the Pomeron production mentioned above.

The first study of the hybrid meson decays $1^{-+} \to \pi b_1$ and πf_1 has recently been made in lattice QCD [27] and shows features that had been anticipated in flux-tube models [36–38]. The flux-tube model has successfully described transitions among conventional mesons [39], and also been applied to the decays of hybrid mesons. A notable feature of the latter, which also emerges in some other models[40, 41], is that the prominent decays are to excited mesons, notably $S + P$ states [36]. This has motivated a possible "explanation" of why such states had not hitherto been seen: multi-pion decays are less well studied. In turn this has directed the strategy for searches.

A particular prediction of the flux tube is that the exotic π_1 is expected to have prominent decays into πb_1 and πf_1, with the former favored by about a factor of four in flux-tube models [36–38]. This result has been confirmed by a lattice computation [27].

Reference [32] has compared the results of the flux tube and lattice QCD and find that near threshold, lattice QCD and flux tube models are in excellent agreement. The results suggest that the spin-dependent features of Strong QCD as revealed by the lattice are contained within the flux-tube model, but that the momentum dependence of the assumed extrapolation differs. When standard intuition about exclusive form factors is consistently included, the implication is that the hybrid widths computed in the flux tube model for decays to asymmetric final states, and for assumed hybrid masses ~ 2 GeV, are consistent with lattice QCD, and that the large widths reported in [27] are likely overestimates. The selection rule that decays to symmetric final states, such as $S + S$, are suppressed, has not yet been tested in lattice QCD. Thus the possibility that hybrid decays occur to e.g. $\pi + \rho$ cannot be ruled out[92]; the prediction that decays to πb_1 exceed πf_1 appears to be robust.

III. LIGHT QUARK SPECTROSCOPY - AN EXPERIMENTAL REVIEW

In this section the experimental searches for exotic hybrid mesons are reviewed, including positive sightings and searches that have produced null results. There have been significant developments since the last GlueX Design Report. We also explore issues in conventional spectroscopy where GlueX can make significant contributions – in the areas of excited vector mesons. The reader is also referred to a comprehensive review of photoproduction [42], a review of light-quark mesons [43] and a review of exotic mesons presented at the 2003 HUGS lectures by E. Klempt [44].

A. Exotic Hybrid Mesons

The emphasis here is not whether certain claims or counter claims are consistent with phenomenological expectations, but rather on the experimental issues. There are of course phenomenological issues inherent in the analyses, for example, interpreting line shapes and phases in terms of a Breit-Wigner parameterization and the specific assumptions that go into amplitude analyses. These are discussed below.

1. $\pi_1(1400) \to \eta\pi$

The first report of evidence for an exotic meson came in 1988 from the GAMS collaboration at CERN using data on the reaction $\pi^- p \to \eta\pi^0 n$ at 100 GeV/c [45]. The purported state had exotic $J^{PC} = 1^{-+}$ with a mass of 1.4 GeV/c^2 decaying into $\eta\pi^0$. The claim for an exotic signal was based on an observed asymmetry in the decay angular distribution as measured in the $\eta\pi^0$ rest frame and was ascribed to the presence of an odd-even wave interference. For an $\eta\pi^0$ system the charge conjugation C is even. Also, $J = L$ and $P = (-1)^L$ where L is the angular momentum between the η and π. Thus a P-wave $\eta\pi$ system has exotic $J^{PC} = 1^{-+}$. Although the purported signal strength was small compared to the dominant D-wave $a_2(1320) \to \eta\pi^0$, it was the interference of the exotic state with the a_2 that supposedly facilitated the detection of the signal. Inconsistencies in the data and analysis were originally pointed out by Tuan, Ferbel and Dalitz [46]. A subsequent re-analysis of the data within the same collaboration called the earlier claim into question [47, 48].

In 1993 the VES collaboration at the IHEP 70 GeV proton synchrotron (Serpukhov) studied data from the reaction $\pi^- N \to \eta\pi^- N$ at an incident momentum of 37 GeV/c. They found a broad $\eta\pi^-$ P-wave enhancement at 1.4 GeV/c^2 [49]. Also in 1993, a group at KEK took data on reaction $\pi^- p \to \eta\pi^- p$ at an incident momentum of 6.3 GeV/c. They also claimed an exotic signal but with a mass and width close to the D-wave $a_2(1320)$ and leakage from this dominant wave into the P-wave could not be excluded [50].

The E852 collaboration published evidence for an exotic $J^{PC} = 1^{-+}$ in the reaction $\pi^- p \to \eta\pi^- p$ [51, 52] in 1997. The P-wave amplitude was described by Breit-Wigner parameters $m = (1379 \pm 16^{+50}_{-30})$ MeV/c^2 and $\Gamma = (385 \pm 40^{+65}_{-105})$ MeV/c^2. The E852 experiment used a 18 GeV/c π^- beam from the Brookhaven Alternating

Gradient Synchrotron into a LH_2 target in the Multiparticle Spectrometer that had been augmented with photon and recoil charged particle detection for E852.

Shortly after the E852 claim, the Crystal Barrel collaboration reported a P-wave $\eta\pi$ wave in the $\bar{p}n$ annihilation channel $\pi^-\pi^0\eta$ with the Breit-Wigner parameters $m = (1400 \pm 20 \pm 20)$ MeV/c^2 and $\Gamma = (310 \pm 50^{+50}_{-30})$ MeV/c^2 [53]. The Crystal Barrel collaboration also later reported that the inclusion of a P-wave $\eta\pi^0$ with the above parameters in describing the channel $\bar{p}p \to \eta\pi^0\pi^0$ was consistent with the claim for the $\pi_1(1400)$ [54].

In 2003, a subset of the E852 collaboration published an analysis of data from the all-neutral final state reaction $\pi^-p \to \eta\pi^0 n \to 4\gamma n$ and found that although a P-wave was present, it could not be described with a Breit-Wigner line shape [55]. The analysis employed here followed closely a prior analysis of the $\pi^-p \to \pi^0\pi^0 n \to 4\gamma n$ reaction [56].

In all the observations in π-induced reactions, the $\eta\pi$ P-wave enhancements have cross sections that are substantially smaller than the dominant $a_2(1320)$, so leakage from this state, usually due to an imperfect understanding of experimental acceptance, is a source of concern. In contrast, the observed yield of the $\pi_1(1400)$ in $\bar{p}p$ annihilations is of the same magnitude as the $a_2(1320)$.

The interpretation of the nature of the low-mass $\eta\pi$ P-wave amplitude and phase motion should be guided by the principle of parsimony – less exotic interpretations need to be considered. For example, in the analysis of the $\eta\pi^0$ E852 data mentioned above, a P-wave is observed but it is not consistent with a Breit-Wigner resonance. The observed P-wave phase motion may be consistent with non-resonant $\eta\pi^0$ final state interactions [57].

2. $\pi_1(1600) \to \eta'\pi$

The E852 collaboration published evidence for a $J^{PC} = 1^{-+}$ exotic meson decaying into $\eta'\pi^-$ with Breit-Wigner parameters $m = (1597 \pm 10^{+45}_{-10})$ MeV/c^2 and $\Gamma = (340 \pm 40 \pm 50)$ MeV/c^2 [58]. Unlike the case for the $\eta\pi$ channel where the D-wave dominates, in this case the P-wave and D-wave are comparable in strength. The phase motion (see Figure 3) is also consistent with resonant behavior. Earlier the VES collaboration [49] reported on the analysis of the reaction $\pi^-N \to \eta'\pi^-N$ and also found that the P-wave dominates the $\eta'\pi^-$ system.

There is also evidence for a P-wave exotic $\eta'\pi$ state in the $\bar{p}p$ channel $\eta'\pi^+\pi^-$ with a mass of 1555 ± 50 MeV/c^2 and a width of 468 ± 80 MeV/c^2 [59].

The interesting and tantalizing aspect of the $\eta'\pi$ system is that the P-wave is large and since competing waves, like the D-wave, are not dominant, issues of leakage in the amplitude analysis may be minimized. It has been speculated that the source of the P-wave is partly due to non-resonant scattering but the inclusion of a narrow exotic resonance cannot be ruled out [57]. Given that this state has been seen in three different experiments, it will be very interesting to look for the photoproduction of this state in GlueX.

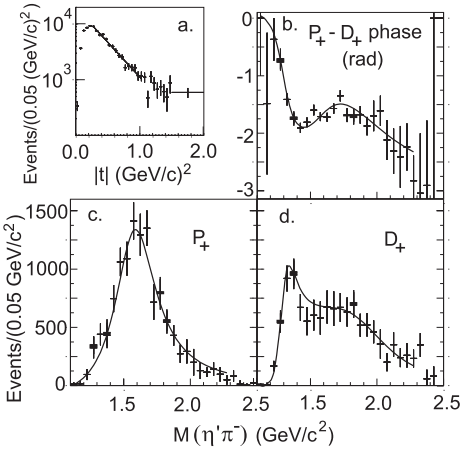

FIG. 3: E852 results of the PWA of the reaction $\pi^-p \to \eta'\pi^-p$ [58]. (a) momentum transfer squared from the incoming π^- to the outgoing $\eta'\pi^-$ system; (b) $P_+ - D_+$ phase; (c) P_+ amplitude and (d) D_+ amplitude.

3. $\pi_1(1600) \to \rho\pi$

In previous versions of the GlueX Design Reports, the E852 claim of a $J^{PC} = 1^{-+}$ exotic meson decaying into $\rho\pi$ [60] was cited as the most robust evidence to date for an exotic meson. This result came from a partial wave analysis of the reaction $\pi^-p \to \pi^-\pi^-\pi^+p$. The reported resonance parameters of the exotic state are $m = (1593 \pm 8^{+29}_{-47})$ MeV/c^2 and $\Gamma = (168 \pm 20^{+150}_{-12})$ MeV/c^2. These parameters were obtained from the interference of the exotic 1^{-+}-wave with the 2^{-+} wave. Confidence in this result was based in part by the fact that the amplitude analysis resulted in observation of well-known states such as the $a_1(1260)$, $a_2(1320)$, $\pi_2(1670)$, $\pi(1800)$ and the $a_4(2040)$ [61]. The fact that the reported exotic width is relatively narrow, coupled with the mass being more in line with expectations from models and LQCD, also helped give some credence to this result. However, the VES collaboration [62] does not find evidence for this state in the reaction $\pi^-N \to \pi^-\pi^-\pi^+N$.

The 3π system with non-zero charge has isospin $I > 0$, and, since no flavor exotic mesons have been found, we assume $I = 1$. Since a state with an odd number of pions has negative G parity, the relationship $G = C(-1)^I$ implies positive C parity for the $(3\pi)^-$ system.

In what follows we will summarize results of a recent analysis of an expanded 3π data set from E852 that also finds no evidence for this state. We present this with enough detail to point out the importance of understanding the biases that can be introduced in an amplitude analysis.

The original E852 analysis was based on 250,000 events

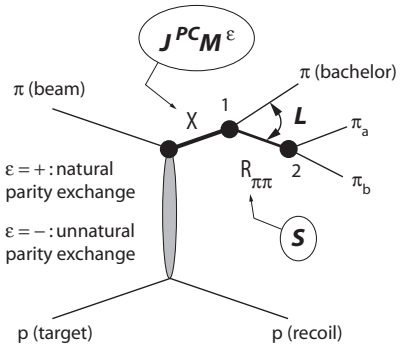

FIG. 4: Partial wave analysis of the 3π system in the isobar model. The state X is characterized by spin (J), parity (P) and charge conjugation (C). It decays at point 1 into a di-pion resonance $R_{\pi\pi}$ (the isobar) and a bachelor π. The di-pion has spin S. The angular momentum between the isobar and the bachelor π is L. At point 2 the di-pion resonance decays into π_a and π_b.

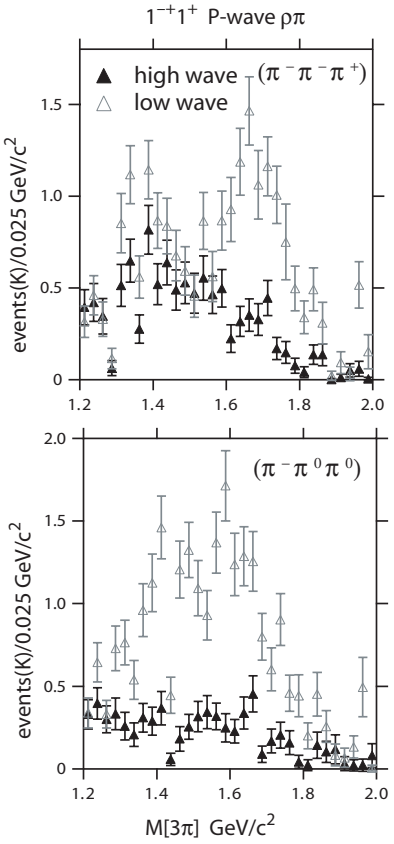

FIG. 5: The $J^{PC} = 1^{-+}$ $\rho\pi$ wave for PWA fits carried out using the high-wave set and low-wave set. Please see the text for details.

of the reaction $\pi^- p \to \pi^-\pi^-\pi^+ p$ collected in 1994. A recent publication [63] reported on the analysis of additional E852 data collected in 1995 including 3.0M events of the reaction $\pi^- p \to \pi^-\pi^0\pi^0 p$ and 2.6M events of the reaction $\pi^- p \to \pi^-\pi^-\pi^+ p$.

In almost all of the published amplitude analyses of the 3π system, including the E852 analysis, the *isobar* model was employed – a 3π system with a particular J^{PC} is produced and decays into a di-pion resonance with well-defined quantum numbers and a bachelor π followed by the decay of the di-pion resonance (see Figure 4). This assumption is successful in describing many features of the 3π system and is motivated by the observation that the di-pion effective mass spectrum shows prominent resonance production, for example, the $\rho(770)$ and the $f_2(1270)$.

In order to extract reliable information from a partial wave analysis it is important to establish a procedure for determining a sufficient set of partial waves. Failure to include important partial waves in the series expansion may lead to inconsistent results and erroneous conclusions. The recent analysis of additional E852 data [63] included a study of the effect of removing individual partial waves on the quality of the fit and a comparison of moments as calculated from PWA solutions with those computed directly from data. The recent analysis is also similar to that of the earlier E852 analysis [60, 61] in that the same isobar model assumptions were made *but* the final set of partial waves used is different. Both analyses make the same assumptions about coherence between different partial waves. It is possible that relaxing these coherence assumptions could lead to different results in both analyses.

In the new analysis a parent set of partial waves (referring to the notation of Figure 4) was defined to include waves with $J \leq 4$, $M \leq 1$ and $S \leq 3$. The $\pi\pi$ isobars included in this analysis are the σ, $f_0(980)$, $\rho(770)$, $f_2(1275)$ and $\rho_3(1690)$, where σ is meant to indicate a S-wave $\pi\pi$ system as described in [61]. In addition, a background wave is included. The background wave is characterized by a uniform distribution in the relevant decay angles and is added incoherently with the other waves.

Waves were sequentially removed from the parent set and the change in likelihood ($\mathcal{L}$) was examined and used as the criterion for either keeping or dropping the wave. The exotic waves would have been removed by this selection criterion but were kept because the existence of signals in these waves was under consideration.

Based on these criteria the compiled set included 35 waves and a background wave – this is the *high-wave set*. The analysis reported in reference [61] used a wave set consisting of 20 waves including the background wave – this is the *low-wave set*.

The results of the analysis with these two wave sets give similar results for dominant waves, such as the $a_2(1320)$ and the $\pi_2(1670)$. Moreover, the relative yields in the two modes, $\pi^-\pi^-\pi^+$ and $\pi^-\pi^0\pi^0$, were consistent with expectations based on isospin. However, the two wave sets yield different results for the exotic wave, as shown in Figure 5.

Using the high-wave set yields a line shape for the

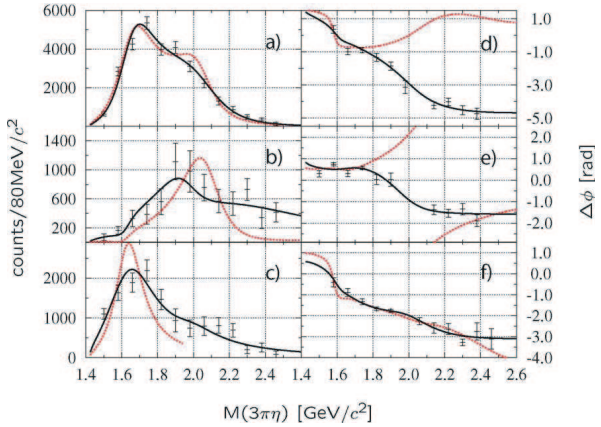

FIG. 6: From reference [64]: results of a PWA of the $\eta 3\pi$ system. $f_1\pi$ intensities of the (a) $1^{-+}0^+(f_1\pi)P$; (b) $2^{-+}0^+(f_1\pi)D$; (c) $1^{-+}1^+(f_1\pi)S$; and phase differences: (d) $\phi(1^{-+}) - \phi(2^{-+})$; (e) $\phi(1^{-+}) - \phi(1^{++})$; and (d) $\phi(1^{++}) - \phi(2^{-+})$. The results from a least squares fit are overlaid as the solid line (two poles in the $1^{-+}f_1\pi$ wave) and the dashed line (one pole). Please reference [64] for details.

charged mode that agrees with the earlier E852 result of reference [61] but using the high-wave set yields no enhancement in the exotic wave amplitude. Furthermore, these studies indicate that leaving out the partial waves corresponding to decay modes of the $\pi_2(1670)$ (P-wave $\rho\pi$ and F-wave $\rho\pi$ - included in the high-wave set but not the low-wave set) leads to a false enhancement in the exotic 1^{-+} wave.

All this underscores the importance of not only understanding experimental acceptance issues but also understanding the systematic biases in the analysis procedure by having an incomplete wave set. Studies are also underway to understand other possible biases introduced by coherence assumptions and mechanisms beyond the isobar model.

4. *Exotic Hybrids Decaying into $b_1\pi$ and $f_1\pi$*

The E852 collaboration has recently published evidence for additional exotic states, all with $J^{PC} = 1^{-+}$. Two states, with masses of 1.6 and 2.0 GeV/c^2, decay into $f_1\pi$ followed by $f_1 \to \eta\pi\pi$ [64] (see Figure 6). Another two states, also with masses of 1.6 and 2.0 GeV/c^2, decay into $b_1\pi$ followed by $b_1 \to \omega\pi$ [65] (see Figure 7). Evidence from VES also finds evidence for $J^{PC} = 1^{-+}$ states with a mass of 1.6 GeV/c^2 decaying into $f_1\pi$ and $b_1\pi$ [62].

These states are intriguing because the higher mass states are in line with theoretical predictions and the decay modes into S-wave plus P-wave $q\bar{q}$ states are those favored by the flux-tube model. However, these states need confirmation.

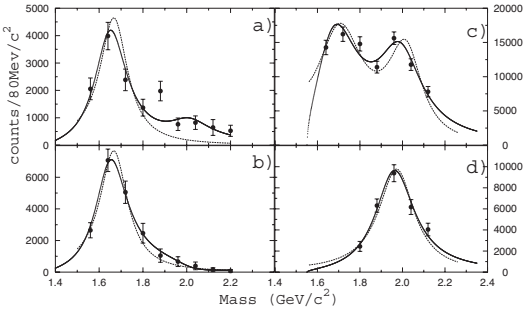

FIG. 7: From reference [65]: results of a PWA of the $\omega\pi\pi$ system. Wave intensities of the (a) $1^{-+}1^+(b_1\pi)$; (b) $1^{-+}0^-(b_1\pi)$; (c) $2^{++}1^+(\omega\rho)$ and (d) $4^{++}1^+(\omega\rho)$. The solid line is the Breit-Wigner result for two 1^{-+} poles and the dashed line is for one. Please reference [65] for details including phase plots.

5. *Exotic Hybrids and GlueX*

GlueX will build on the pioneering work of the experiments that have pointed to channels that have tantalizing signals for exotic mesons. It is clear that amplitude analyses are needed to extract information about these states and that high quality data with excellent resolution and acceptance and high statistics are essential. The GlueX detector is optimized for such analyses. It is also clear that it is important to do careful self-consistency checks in applying the amplitude analyses so as to avoid biases that could give rise to incorrect conclusions. Finally, GlueX will use a photon probe, that, as pointed out above, is likely to be more efficient at producing exotic hybrid mesons compared to pion probes.

B. Conventional Light Quark Meson Spectroscopy

The primary focus of GlueX is mapping the spectrum of exotic hybrid mesons, but this mapping necessarily requires mapping the spectrum of conventional mesons as well. By *conventional* we mean mesons that are members of the light quark $q\bar{q}$ nonets. As is evident from the above discussion of the amplitude analysis of the 3π system, the analysis identifies states not only by their line shapes in intensity but also through their interference with other states (usually conventional mesons) nearby in mass. So in the process of doing the analysis to identify the exotic states, the high quality data to be collected by GlueX will yield important information about the light quark meson spectrum.

The reader is reminded that in the conventional quark model the three light quarks form flavor SU(3) nonets characterized by a given set of J^{PC} quantum numbers that are in turn determined by the relative orbital angular momentum (L) between the quarks and the relative orientation of their spins (parallel or anti-parallel). Three members of the nonet have isospin $I = 1$, four have $I = \frac{1}{2}$ and two have $I = 0$. The $I = \frac{1}{2}$ members have

TABLE I: Map of the ground state mesons up through $L = 5$. (Some of these assignments are not without controversy).

$n^{2s+1}L_J$	J^{PC}	$I=1$ $u\bar{d}\cdots$	$I=\frac{1}{2}$ $u\bar{s}\cdots$	$I=0$ f^a	$I=0$ f'^a
1^1S_0	0^{-+}	π	K	η	η'
1^3S_1	1^{--}	ρ	K^*	ω	ϕ
1^1P_1	1^{+-}	$b_1(1235)$	K_{1B}	$h_1(1170)$	$h_1(1380)$
1^3P_0	0^{++}	$a_0(1450)$	$K_0^*(1430)$	$f_0(1370)$	$f_0(1710)$
1^3P_1	1^{++}	$a_1(1260)$	K_{1A}	$f_1(1285)$	$f_1(1420)$
1^3P_2	2^{++}	$a_2(1320)$	$K_2^*(1430)$	$f_2(1270)$	
1^1D_2	2^{-+}	$\pi_2(1670)$	$K_2(1770)$	$\eta_2(1645)$	$\eta_2(1870)$
1^3D_1	1^{--}	$\rho(1700)$	$K^*(1680)$	$\omega(1650)$	
1^3D_2	2^{--}		$K_2(1820)$		
1^3D_3	3^{--}	$\rho_3(1690)$	$K_3^*(1780)$	$\omega_3(1670)$	$\phi_3\prime(1850)$
1^1F_3	3^{+-}				
1^3F_3	3^{++}				
1^3F_4	4^{++}	$a_4(2040)$	$K_4^*(2045)$	$f_4(2050)$	
1^3F_5	5^{++}				
1^1G_4	4^{-+}				
1^3G_4	4^{--}				
1^3G_5	5^{--}	$\rho_5(2350)$			
1^3G_6	6^{--}				
1^1H_5	5^{+-}				
1^1H_4	5^{++}				
1^3H_6	6^{++}	$a_6(2450)$		$f_6(2510)$	
1^1H_7	7^{++}				

[a] f and f' are linear combinations of the SU(3) flavor octet and singlet states.

TABLE II: Map of the Radial Excitations. (Except for the top two rows, these assignments are speculative).

$n^{2s+1}L_J$	J^{PC}	$I=1$ $u\bar{d}\cdots$	$I=\frac{1}{2}$ $u\bar{s}\cdots$	$I=0$ f^a	$I=0$ f'^a
2^1S_0	0^{-+}	$\pi(1300)$	$K(1460)$	$\eta(1295)$	$\eta(1475)$
2^3S_1	1^{--}	$\rho(1450)$	$K^*(1410)$	$\omega(1420)$	$\phi(1680)$
2^1P_1	1^{+-}			$h_1(1595)$	
2^3P_0	0^{++}				
2^3P_1	1^{++}	$a_1(1640)$			
2^3P_2	2^{++}	$a_2(1700)$		$f_2(1810)$	
3^1S_0	0^{-+}	$\pi(1800)$		$\eta(1760)$	
3^3S_1	1^{--}	$\rho(1900)$			

[a] f and f' are linear combinations of the SU(3) flavor octet and singlet states.

non-zero strangeness. The two $I = 0$ members (f and f') are linear combinations of the SU(3) flavor octet and singlet states. In some cases (1^{--}, 2^{++},3^{--}) these combinations are *ideally mixed* with one state nearly pure $s\bar{s}$ (*e.g.* $\phi(1020)$) and the other with no strange component (*e.g.* $\omega(780)$). In Table I we show the map of the ground state light quark mesons up through $L = 5$. Note the missing states and also note that the mass range is within the reach of GlueX.

In addition to the ground state nonets, radial excitation are possible within the conventional quark model. In Table II we show the map of the light quark radial excitations.

We now will focus on the excited vector mesons.

C. Excited Vector Mesons

Why study the photoproduction of excited light quark vector mesons? First of all, in both the light and heavy quark sectors the ground state vector mesons ($1\ ^3S_1\ q\bar{q}$), *i.e.* the ρ, ω, ϕ, J/ψ and Υ, are well understood. An understanding of how the light quark and heavy quark sectors connect is important if we are to eventually understand the light quark sector in mapping gluonic excitations – *glueballs* and *hybrid* mesons. The vector mesons are thus ideal for providing this connection. From a study of their decays in ϕ, J/ψ and Υ factories, much has been learned about QCD hadronic physics. The ground state light quark vector nonet is very well understood. The flavorless members of this nonet, the ω and ϕ, are nearly ideally mixed so that ϕ is essentially composed entirely of s quarks and the ω entirely of u and d quarks. Within the quark model we expect excitations of the ground state vectors and these include both radial ($2\ ^3S_1$) excitations and orbital ($1\ ^3D_1$) excitations. In the heavy quark sector these vector excitations are well mapped and studied. But the situation in the light quark sector is at best murky, as will be discussed below.

It has also been speculated [66] that the radiative decays of excited vector mesons can be used to provide unique information about their decay products and to isolate evidence for mesons with gluonic degrees of freedom.

In the heavy quark sector the vectors are produced in e^+e^- collisions. In the light quark sector much of the information we have on possible excited vector states also comes from e^+e^- collisions. But the measurements of the masses, widths and decay modes of reported states are inconsistent. Photoproduction is complementary to e^+e^- collisions and may be better suited to understanding the light quark excited vectors. One advantage of producing states directly in e^+e^- collisions is that one starts with a clean $J^{PC} = 1^{--}$ initial state. On the other hand photoproduction allows for other J^P states. This could be viewed as a virtue since it allows one to exploit interference with well-known states to help establish new states.

The elastic photoproduction of the ground state vector mesons, ρ, ω and ϕ has been well studied. Within the Vector Dominance Model (VDM) picture the photon fluctuates into a virtual $1\ ^3S_1\ q\bar{q}$ (vector meson V) that elastically scatters off of the proton resulting in $\gamma p \to Vp$. Of course the photon can also fluctuate into a virtual $2\ ^3S_1$ or $1\ ^3D_1\ q\bar{q}$ (excited vector V^*) followed by elastic scattering of the excited vector resulting in $\gamma p \to V^* p$.

Our current information about the excited vector mesons comes from e^+e^- collisions with only a few results from hadro- and photoproduction and τ decays [67]. There is general agreement about the existence of these excited isovector-vector mesons ($\rho(1450)$ and $\rho(1700)$), the excited isoscalar-vector mesons ($\omega(1420)$ and $\omega(1650)$) and the excited isoscalar-vector with hidden strangeness ($\phi(1680)$). There are, however, inconsistencies in the masses, widths and decay modes. For example, the quoted masses for the $\rho(1450)$ range from 1290 ± 40 to 1582 ± 25 MeV/c^2 while the quoted widths range from 60 ± 15 to 547 ± 86 MeV/c^2. Masses and widths for the other excited vector states show similar inconsistencies. Many of the decay modes allowed by quantum number conservation are merely listed as *seen* in the Review of Particle Physics (RPP) [67]. The 2004 RPP has a review [68] of the $\rho(1450)$ and $\rho(1700)$. In the 1988 version of the RPP there was a single excited ρ – the $\rho(1600)$ which has been superseded by the $\rho(1450)$ and $\rho(1700)$. There is also a report of a photoproduced $\bar{K}K$ state with a mass of 1750 MeV/c^2 [69] by the FOCUS collaboration.

Separately, and with co-workers, A. Donnachie has reviewed the experimental situation with excited vector mesons [70–73]. The disparity among various experiments with regard to the properties of excited vector mesons, alluded to above, highlights why these states are of great interest. Further experiments are needed to learn about the substructure of these states. A comparison of e^+e^- data, τ decays and photoproduction is essential.

GlueX is ideally suited to provide the critical data needed for a full mapping of excited vector mesons. GlueX will increase the current statistics on light quark photoproduction by several orders of magnitude. Many of the current inconsistencies will be removed by doing a proper amplitude analysis for a variety of decay modes.

IV. GLUEX REQUIREMENTS FOR THE ELECTRON AND PHOTON BEAMS

A. Overview

Much of this section is extracted from two technical notes: `GlueX-doc-389` and `GlueX-doc-646` that are available for PAC members on the web site `www.gluex.org`.

Our guidance for the masses of the low-lying exotic hybrid nonets, and the mass splittings among the nonets, comes from LQCD. The masses and splittings depend on the gluonic degrees of freedom. For example, the SESAM collaboration predicts that the exotic hybrids involving u and d quarks alone have masses of 2.3 ± 0.6, 1.9 ± 0.2 and 2.0 ± 0.1 GeV/c^2 respectively for the 0^{+-}, 1^{-+} and 2^{+-} nonets [74]. The $s\bar{s}$ members are expected to be typically 0.2 to 0.3 GeV/c^2 more massive. Keeping in mind that mapping the spectrum of exotics involves identification of the nonet members, GlueX needs a mass reach of up to approximately 2.8 GeV/c^2.

This mass reach requires a photon beam energy of 9 GeV – well enough above threshold for the meson mass range of interest to ensure that the mesons have sufficient boost so that their decay products are detected with sufficient precision and also so line shape distortions due to kinematic and dynamic effects are minimized.

Linearly polarized photons are required for the amplitude analyses needed to extract information about the spin-parity of produced mesons. The optimal technique for producing linearly polarized photons for GlueX is coherent bremsstrahlung. In order to obtain the required degree of linear polarization for a given photon energy, it is essential that the electron energy be sufficiently high (12 GeV in this case) and that the photon beam be collimated. The ability to collimate in turn depends on having a sufficiently thin diamond wafer radiator (≈ 20 μm) and a sufficiently small electron beam emittance (10 mm·μr). The GlueX experiment is unique among Jefferson Lab experiments in that its required emittance is close to the ideal limits of the machine.

Figure 8 shows the flux of incoherent and coherent bremsstrahlung radiation off of a diamond radiator with incident 12 GeV electrons where the diamond is oriented to yield a coherent photon energy peak at 9 GeV. The spectrum before and after collimation is shown. Also shown is the region of tagged photons – it is this range of photons that will be used to do the physics of GlueX. The width of the peak is about 0.6 GeV with a maximum photon energy of 9 GeV.

For a fixed electron energy the diamond crystal can be rotated relative to the electron beam to move the position of the coherent peak. The average linear polarization of the photons in the tagged peak decreases as the photon peak energy moves closer to the electron energy.

B. Meson Masses and Photon Beam Energy

In order to understand the importance of the photon beam energy in reaching the desired meson masses we will assume three possible photon coherent peak positions: 8, 9 and 10 GeV each with a width and shape roughly given by the spectrum in the tagging range of Figure 8.

Consider the production of meson X in the reaction $\gamma p \to Xp$. The four-momenta of the particles in the reaction are p_γ, p_{p_t}, p_X and p_{p_r} (where p_t and p_r are the target and recoil protons). The kinematics of this reaction are characterized by the center of mass energy squared, s, and the momentum transfer squared, t, from

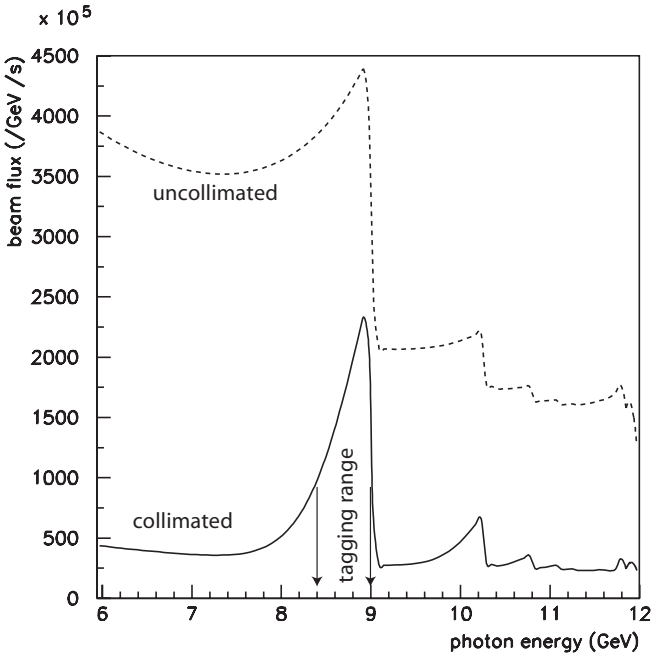

FIG. 8: Flux of incoherent and coherent bremsstrahlung radiation off of a diamond radiator with incident 12 GeV electrons where the diamond is oriented to yield a coherent photon energy peak at 9 GeV. The spectrum before and after collimation is shown. Also shown is the region of tagged photons.

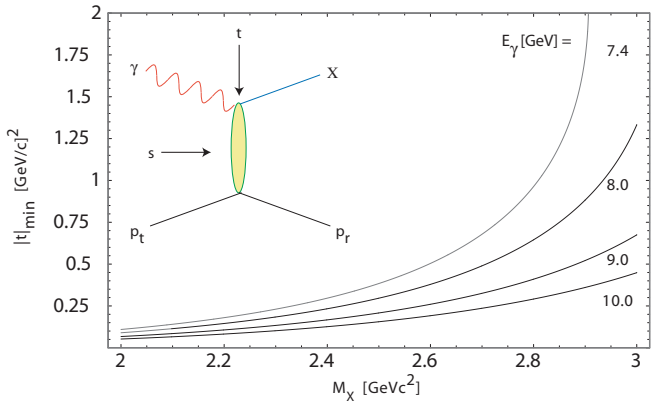

FIG. 9: Dependence of the minimum value of $|t|$ as a function of M_X for the reaction $\gamma p \to Xp$. The inset diagram shows the peripheral production of X with arrows indicating the variables $s = (p_\gamma + p_{p_t})^2$ and $t = (p_X - p_\gamma)^2$ in terms of the relevant four-momenta and where p_t and p_r refer to the target and recoil protons respectively. The curves correspond to beam photon energies, E_γ, of 8.0 GeV, 9.0 GeV and 10.0 GeV. The curve at 7.4 GeV is shown because that is the lower edge of the photon energy range defined by the 8.0 GeV peak.

the incident photon to the produced meson X. In terms of the four-momenta $s = (p_\gamma + p_{p_t})^2 = m_p(m_p + 2E_\gamma)$ and $t = (p_X - p_\gamma)^2 = (p_{p_t} - p_{p_r})^2$.

For beam photon energies greater than a few GeV the production of mesons is predominantly peripheral as indicated by the diagram in the inset of Figure 9. The

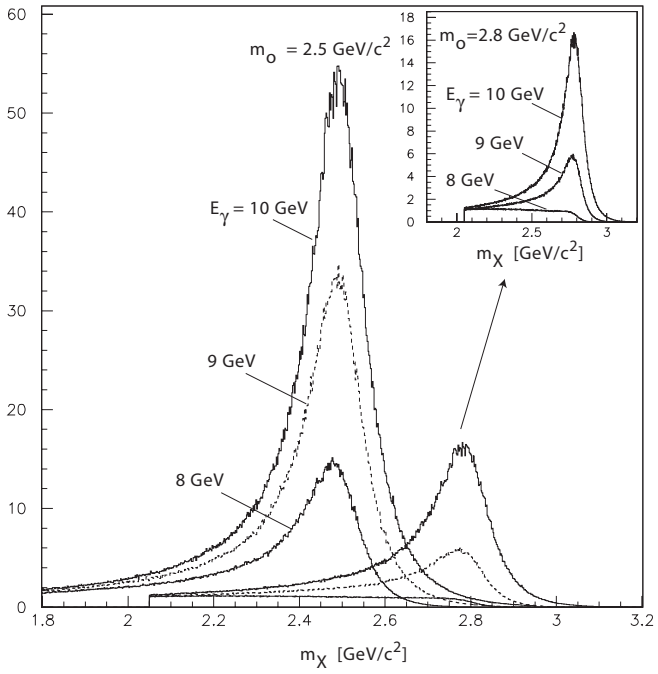

FIG. 10: Breit-Wigner line shape for resonances of masses of 2.5 and 2.8 GeV/c^2 weighted by an amplitude that falls exponentially in $|t|$ with a slope parameter of $\alpha = 8$ (GeV/c)$^{-2}$. The resonance width is assumed to be 0.15 GeV/c^2. For each resonance the yield is shown for photon peak energies of 10, 9 and 8 GeV. The inset shows the yield for the 2.8 GeV/c^2 energy in more detail.

distribution in $|t|$ falls off rapidly with a typical dependence characterized by $e^{-\alpha|t|}$ where for this study we assume a typical value of $\alpha \approx 8$ (GeV/c)$^{-2}$. As the central mass m_X of the resonance approaches the kinematic limit $(\sqrt{s} - m_p)$ for the production of the resonance the minimum $|t|$, $|t|_{min}$, needed to produce the resonance rises rapidly with m_X and has a significant variation across the width (Γ) of the resonance. This distorts the line shape and decreases the integrated yield. In Figure 9 we show the dependence of $|t|_{min}$ as a function of m_X. The curves correspond to beam photon energies, E_γ, of 8.0 GeV, 9.0 GeV and 10.0 GeV. The curve at 7.4 GeV is shown because that is the lower edge of the photon energy range defined by the 8.0 GeV peak. So the variation of $|t|_{min}$ with M_X is indeed very rapid above $\approx$ 2.6 GeV/c^2 for the 8.0 GeV peak.

In Figure 10 we show the Breit-Wigner line shape and overall production rate for resonances of masses 2.5 and 2.8 GeV/c^2 are affected by the value and variation of $|t|_{min}$ across the width of the resonance for various assumptions about the position of the coherent photon peak. We assume the same cross-section for the two resonances and describe the line shape by a Breit-Wigner form weighted by an amplitude that falls exponentially in $|t|$ with a slope parameter of $\alpha = 8$ (GeV/c)$^{-2}$. The resonance width is assumed to be 0.15 GeV/c^2. For each

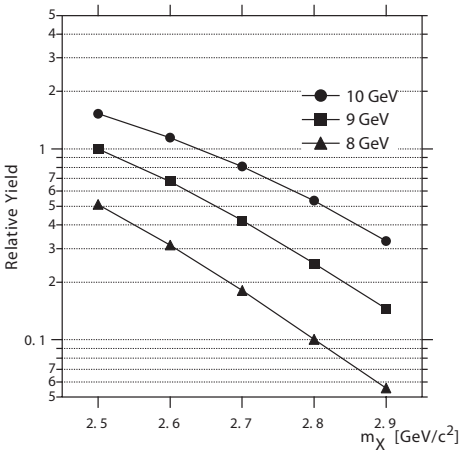

FIG. 11: Relative yield as a function of meson mass for beam photon peak energies of 8, 9 and 10 GeV. The variation in yield is due to the exponential fall off of production as a function of $|t|$ combined with the variation of $|t|_{min}$ with M_X as explained in the text.

of the two resonances we show how the line shape and yield change as the tagged photon peak moves from 10 to 9 to 8 GeV. The inset shows this variation for the resonance of mass 2.8 GeV/c^2 in more detail. It can be seen that the line shape varies dramatically as the photon peak moves from 10 to 9 to 8 GeV. And in the step from 9 to 8 GeV, for the resonance at 2.8 GeV/c^2, the resonance shape disappears.

Figure 11 shows the relative yield of resonances as a function of mass for beam photon peak energies of 8, 9 and 10 GeV with the assumptions described above. The conclusion from this study is that lowering the tagged photon beam energy for GlueX would have a severe negative impact on the discovery potential for this experiment.

C. Linear Polarization and Analysis

The amplitude analysis that will be employed by GlueX to identify the spin, parity and charge conjugation quantum numbers of produced meson states and their production mechanisms depends critically on having linearly polarized photons. Significant pioneering work on the photoproduction of mesons was carried out at SLAC, near proposed GlueX photon energies, using a low-intensity linearly polarized photon beam produced by Compton backscattering off of laser light [75] into a liquid hydrogen bubble chamber.

Consider photon beams that are (1) unpolarized; (2); circularly polarized with either $|R\rangle$ or $|L\rangle$ polarization; or (3) linearly polarized with $|x\rangle$ or $|y\rangle$. The linear polarization states are related to the circular states by $|x\rangle = (|L\rangle - |R\rangle)/\sqrt{2}$ and $|y\rangle = i(|L\rangle + |R\rangle)/\sqrt{2}$. From this we can see how maximal information from decays are obtained with linearly polarized photons, as opposed

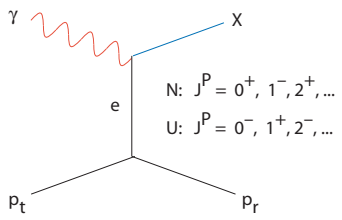

FIG. 12: Photoproduction of a meson X by the exchanged of a particle e with natural (N) or unnatural (U) parity.

to unpolarized or circularly polarized photons.

Consider the diagram of Figure 12 that shows the photoproduction of a meson X via exchange of a particle (e) with either natural (N) or unnatural (U) parity. Natural parity for the exchange particle assumes that the spin J_e and parity P_e are related by $P_e = (-1)^{J_e}$ whereas for unnatural parity $P_e = (-1)^{J_e+1}$.

The wave function for $X \to a + b$, if the spin of X is ℓ, is given by $Y_\ell^m(\theta, \phi)$ where $m = \pm 1$. If the photon is circularly polarized with either $m = \pm 1$ then the observed decay angular distribution is given by $W(\theta, \phi) = |Y_\ell^{\pm 1}(\theta, \phi)|^2 \propto |P_\ell^1[\cos\theta] e^{\pm i\phi}|^2 \propto (P_\ell^1[\cos\theta])^2$. If the photon is linearly polarized then for $|x\rangle$ polarization the wave function is proportional to $Y_\ell^{+1} - Y_\ell^{-1}$ yielding $W(\theta, \phi) \propto (P_\ell^1[\cos\theta])^2 \cos^2\phi$ whereas for $|y\rangle$ polarization the wave function is proportional to $Y_1^{+1} + Y_1^{-1}$ and $W(\theta, \phi) \propto (P_\ell^1[\cos\theta])^2 \sin^2\phi$. With unpolarized photons or circularly polarized photons there is no information from the ϕ decay angle – that only occurs in the case of linear polarization.

Polarization information can also be used to separate meson production by natural (N) or unnatural (U) parity exchange. For example, diffractive photoproduction, which occurs by Pomeron exchange (natural parity exchange), will produce background to exotic meson production that may occur through unnatural parity exchange. With unpolarized photons or circularly polarized photons the two exchange processes cannot be isolated. But with linear polarization, the two exchange mechanisms can be separated by selecting events based on the angle that the polarization vector makes with the production plane. This was originally pointed out in papers by Cooper [76] and Thews [77] and developed more fully shortly thereafter in a detailed treatment by Schilling, Seyboth and Wolf [78] who present distributions including those for partial linear polarization. This ability to select the production mechanism was exploited by Afanasev and Szczepaniak [79] who point out that a similar selection can be used as an *exotics filter* mechanism.

D. Electron Beam Energy & Emittance

Electron beam energy is an important beam property for achieving the physics goals of GlueX. For 9 GeV photons, the polarized beam intensity and polarization are

strongly dependent on electron beam energy. Beam intensity is controlled by electron beam current, so the reader may wonder how this is coupled to the beam energy. The reason for this is tied to the presence of all of the low-energy photons that are present in the photon beam together with the tagged photons at 9 GeV. At the low-energy end of the photon beam spectrum the spectral intensity scales like $1/k$ where k is the photon energy, so in terms of photon count, the beam is dominated by low-energy photons. These low-energy photons undergo both electromagnetic and hadronic interactions in the target which are the primary source of background in the detector. The GlueX detector and trigger are designed to operate in the presence of these backgrounds and ignore them, but there are limits on how high a background is acceptable. Independent of what those exact limits will be, it is possible to compute a relative figure-of-merit as a function of electron beam energy.

The polarization figure-of-merit is the product of the intensity of the tagged photon beam at the entrance to the GlueX target multiplied by its mean-square linear polarization. More precisely,

$$fom = \int_{E_0}^{E_1} \frac{dN}{dE} P^2(E)\, dE \qquad (1)$$

where dN/dE is the spectral intensity of the collimated photon beam, $P(E)$ is its linear polarization, and E_0 and E_1 are the limits of the tagged region of the spectrum.

The results are shown in Figure 13 for a variety of collimator diameters located 75 m downstream of the tagger. These curves were generated by computing the square of the average polarization in the photon beam multiplied by the flux of tagged photons between 8.4 and 9 GeV divided by the total hadronic interaction rate in the target. Each curve is a smooth interpolation between points at several discrete energies over the range 9 - 13 GeV. Normalizing to the total electromagnetic rate instead of the hadronic rate would produce essentially the same result. The lowest curve in the figure corresponds to the photon beam without any collimator in place. It is included to show that the improvement in the beam polarization figure-of-merit in going from 9 GeV to 12 GeV electrons is mainly achieved through collimation.

The electron beam emittance at the entrance to the crystal radiator is very important to the GlueX experiment. Having a small-emittance electron beam, along with a thin (20 μm) diamond radiator, is what makes it possible to use strict collimation to significantly enhance the photon beam 9 GeV flux and polarization. Both the tagging efficiency and the polarization figure-of-merit are sensitive to emittance. The combined figure-of-merit, taking into account both tagging efficiency and polarization figure-of-merit, as a function of electron beam emittance are shown in Figure 14 for various collimators. The combined figure-of-merit falls steeply above an emittance of 10 mm·μr, showing that the experiment is significantly degraded if the emittance degrades beyond this point.

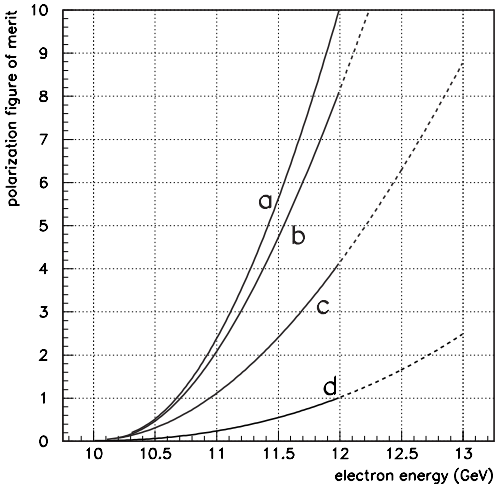

FIG. 13: Polarization figure-of-merit (arb. units) as a function of electron beam energy for the reference design with (a) a 1.6 mm diameter collimator, (b) a 3.2 mm diameter collimator, (c) a 6.4 mm diameter collimator, and (d) without a collimator. The vertical axis has been normalized to unity for an uncollimated beam at 12 GeV. The reference configuration is represented by the intersection of curve (b) with the vertical grid line at 12 GeV.

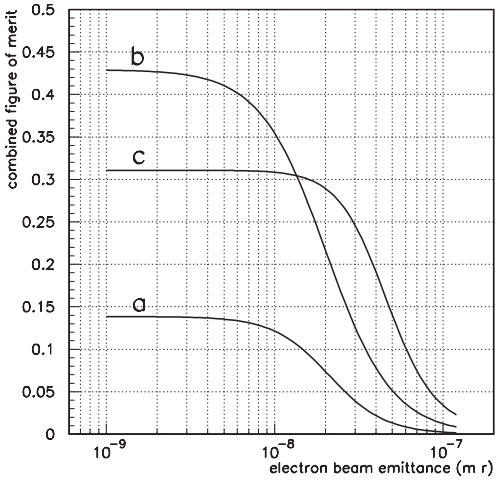

FIG. 14: Combined figure-of-merit as a function of horizontal electron beam emittance for (a) a 1.6 mm diameter collimator, (b) a 3.2 mm diameter collimator, and (c) a 6.4 mm diameter collimator. The tagging efficiency and polarization figure-of-merit were combined by simply taking their product. The reference configuration is represented by the intersection of curve (b) with the vertical grid line at 10^{-8} m·r.

E. Summary

The discovery potential of GlueX depends critically on the photon beam energy ($8.4 - 9$ GeV) and degree of linear polarization ($\approx 40\%$) and these in turn require an electron energy of at least 12 GeV and a maximum horizontal emittance of 10 mm·μr.

V. THE GLUEX DETECTOR

A. Overview

The GLUEX detector design is based on optimizing the amplitude analysis needed to extract information about quantum numbers of meson states. The amplitude analysis is applied to exclusive processes. Kinematical identification of exclusive processes requires a detector with excellent energy resolution and particle identification. Excellent and well-understood acceptance is also essential. Finally, the detector must have the rate capability to handle the event rate needed to carry out the high statistics analysis. The detector design as presented to the GLUEX Detector Review Committee in October 2004, along with the report from that committee, are available for PAC30 members on the web site `www.gluex.org`.

B. Detector Simulation

In the initial phases of the GLUEX detector design the collaboration adopted the MCFAST fast tracking simulation package developed at Fermilab for detector design studies [80]. The realization of this package for GLUEX is called HDFAST and included geometrical and resolution information about the tracking chambers, calorimetry and the magnetic field map of the superconducting solenoid. This was used to estimate detector acceptance. For example, Figure 15 shows the acceptance of the GLUEX detector for the photoproduction of meson X in the reaction $\gamma p \to Xp$ for $E_\gamma = 9$ GeV. Three cases are considered: $X \to 3\pi$, $X \to 2\pi\omega$ and $X \to 2\pi\eta$. These final states will be the focus of the first two years of GLUEX detector operation. The acceptance calculations were based on HDFAST estimates of detector resolutions.

The GLUEX collaboration is now in the process of implementing a more realistic GEANT-based simulation and reconstruction package for the detector. The simulation propagates tracks through the detector, generates hits in sensitive materials, and collects the hits at the end of each event into an output record. Representing the detector geometry in a form that is suitable for accurate and efficient simulation requires a model for each detector subsystem. Models have been assembled for each subsystem that satisfy the minimum requirements that they have the correct sensitive area coverage, the right amount and type of material at a level of detail better than the detector position resolution, and at least as much segmentation as required by the readout. Details are given in `GlueX-doc-654.`

This new and more realistic version of the detector simulation is being used to understand charged particle reconstruction. Charged particle tracking in the GLUEX detector will be carried out in several stages. The first stage performs pattern recognition to identify track candidates. These candidates are then fit using a simplified magnetic field model to obtain initial guesses for momentum and vertex positions. This information is then given to a track fitter that incorporates a map of the GLUEX magnetic field as well as material in the tracking volume to obtain the best estimates for the track parameters at the production vertex. Finally, the tracks need to be matched to hits in other detectors in GLUEX, after which a global optimization to the track parameters can be performed.

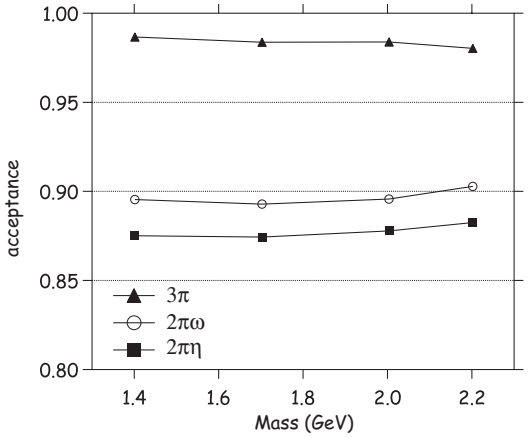

FIG. 15: The acceptance of the GLUEX detector for the photoproduction of meson X in the reaction $\gamma p \to Xp$ for $E_\gamma = 9$ GeV. Three cases are considered: $X \to 3\pi$, $X \to 2\pi\omega$ and $X \to 2\pi\eta$. These final states will be the focus of the first two years of GLUEX detector operation. The acceptance calculations were based on HDFAST estimates of detector resolutions.

Pattern recognition and simplified fitting has been studied in GLUEX. Figure 16 shows a simulated 4-muon event for which the hit positions have been smeared and noise hits added to the detector response. The four muon tracks are reconstructed using software that has been developed for GLUEX. Work is now moving forward on the track fitter that incorporates the magnetic field. This is expected to be based on standard techniques such as Kalman filtering [81, 82]. This latter work will also form the basis of matching tracks to hits in other detectors and the eventual global optimization of tracks. The current status of track-finding is described in `GlueX-doc-658.`

C. Summary of R&D to Date

Based, in part, on the recommendations of the GLUEX Detector Review Report of October 2004, the collaboration has been continuing detector R & D on all subsystems. What follows here is a brief status report and future plans. Detector tests have been carried out using cosmic rays and beams at the Serpukhov accelerator in Russia and the TRIUMF accelerator in Canada. Photon and electron beam tests are planned in HALL B at JLAB starting in September 2006.

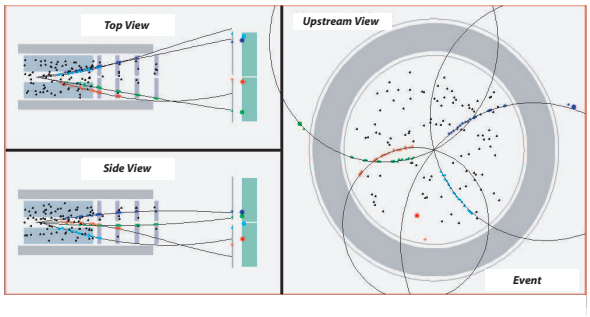

FIG. 16: GEANT-based simulation (including backgrounds) and reconstruction of a 4-muon event in the GLUEX detector CDC (central drift chamber) and FDC (forward drift chamber) systems.

1. Photon Beam

The tagging spectrometer and photon beamline were extensively reviewed in January 2006. Quoting from the Executive Summary of the committee report:

Based on the material presented at the review, the committee has come to the conclusion that the conceptual design of the tagger magnet and the hodoscope systems are well motivated by the Hall D physics goals, and are adequate to achieve those goals. The committee is also convinced that the design parameters of the photon beamline are optimized to achieve the highest possible linear polarization at the envisioned high tagging rates.

Work is in progress to check on the compatibility of using silicon photomultiplier in the design of the tagger hodoscope microscope. The 'pin cushion' active collimator is being designed. Extensive work has been done understanding the backgrounds expected in the tagger building. This work has been done in conjunction with personnel in Radcon (Radiation Control) to provide feedback to those designing the tagger building and beam dump area.

2. UPV

The upstream photon veto (UPV) will be used to detect photons emitted in backwards direction. Simulations indicate that using scintillators with embedded fibers is an attractive option for light collection. Construction techniques are being tested.

3. Start Counter

During the GLUEX detector review, questions were raised regarding the need of a START counter and the effects that the detector material would have on the ultimate vertex resolution. Using GEANT-based simulations contributions to the vertex resolution of a liquid hydrogen target surrounded by a start counter of various thicknesses were studied and described in `GlueX-doc-479`.

Based on these studies and the CLAS experience, it was decided that a simplified version of the START counter with fewer elements will be very useful in the initial stage of the experiment when lower photon beam intensities are used. The START counter will be removed for higher intensity running.

4. BCAL

The barrel electromagnetic calorimeter (BCAL) design is based on the KLOE calorimeter and uses a lead/scintillating fiber matrix. The BCAL calorimeter has to operate inside the high-field (2.2 T) of the superconducting solenoid. R & D is focused on a silicon photomultiplier (SiPM) read out scheme and on fiber tests. A 4 m-long BCAL module will be tested in a photon beam later this year. Another 4 m-long BCAL module is under construction.

The GLUEX collaboration is working with SensL on developing large-area ($\approx$ 1.3 cm^2) SiPM's. These detectors can be placed directly on the end of the BCAL modules and operate inside the solenoid. The first prototypes for testing will be available in July 2006. So far, the technology looks very promising. A back-up plan using micro-channel plate photosensors is also being studied.

The KLOE fibers were supplied by PoliHiTech but this company no longer produces scintillating fibers. Also, the long attenuation length achieved for these fibers came at the expense of sensitivity to damage by visible light. Fast green fibers are now available that are insensitive to visible light, are fast, have a long attenuation length and an emission peak well-matched to photosensors.

The GLUEX collaboration will use one week of beam time delivered to Hall B during the September-October 2006 period when the CEBAF accelerator is running at 687 MeV. The electron beam will produce a photon beam using the Hall B tagger system. Photons of various energies will be used to measure the response of a 4 m-long lead/scintillating fiber (Pb/SciFi) prototype module for the GlueX barrel calorimeter (BCAL). The 687 MeV endpoint energy will provide a range of low-energy photons to study the behavior of the calorimeter at threshold, which presents a special challenge. The module will be mounted on a support system in the Hall B alcove area. The module will be illuminated at several positions along its length and at several angles, from 0° to 80° with respect to normal incidence. These data will allow a measurement of the energy resolution, linearity, time resolution and spatial resolution and will also allow a validation of the Monte Carlo simulations of the calorimeter. A schematic of the the test setup is shown in Figure 17.

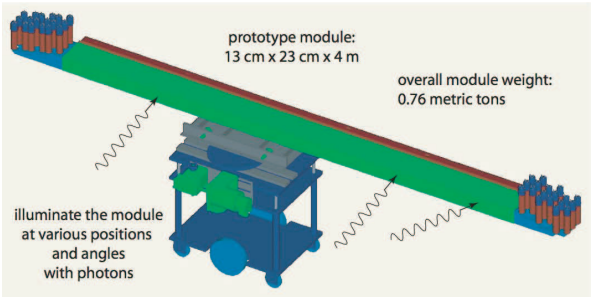

FIG. 17: Schematic of the prototype BCAL module with its proposed readout scheme and support cart.

5. FCAL

The forward calorimeter (FCAL) using lead glass blocks was used in Brookhaven experiment E852 [83, 84] and in the JLAB RADPHI experiment [85]. Based on extensive studies of the energy resolution and π^0 and η mass resolutions, it was determined that a significant improvement in resolution, by a factor of 1.5 to 2.0, could be achieved by using light guides between the lead glass and PMT's to increase the photon collection of each element. Various techniques are being tried and tested with cosmic rays for coupling the lead glass blocks to PMT's. A 64-module FCAL will be tested in HALL B in 2007.

The 2007 beam tests will also include tests of the FDC prototype. The collaboration will prepare a detailed request including beam conditions and beam time for presentation to the JLAB PAC.

6. PID

Particle identification (PID) in GLUEX will use input from nearly all the detector systems in the experiment. Time-of-flight information will be obtained from both the forward TOF system and BCAL. The Čerenkov detector will provide information on forward going tracks, while the central drift chamber (CDC) will provide dE/dx information.

In order to effectively use all of this information, GLUEX plans to develop of likelihood-based PID system. In such a scheme, each detected particle is assigned a probability of being a π, K, p, $\cdots$. These individual probabilities can then be combined with kinematic fitting to perform a global PID using all available information at once. Such a scheme is similar to what was carried out in the Crystal Barrel Experiment at CERN.

7. Čerenkov Counter

Discussions are underway with members of the BABAR Collaboration to explore the possible use of part of the BABAR DIRC as part of the GLUEX PID system. Another possibility is use of a threshold gas Čerenkov counter using C_4F_{10} as a radiator.

8. TOF

Cosmic ray tests and beam tests of time-of-flight (TOF) modules have been carried out at Serpukhov using a 5 GeV hadron beam [86–88]. In these tests various PMT's were tested, along with scintillators from various suppliers and of various dimensions were also tested. Beam tests were also performed at TRIUMF and results are described in `GlueX-doc-634.` Further cosmic tests with thicker scintillator bars and a variety of readout electronics are currently underway.

9. CDC

The central drift chamber (CDC) will be a 1.75 m-long straw-tube drift chamber with 23 layers surrounding the GLUEX target. The chamber will provide $r-\phi$ measurements from timing and z information through the use of stereo layers. A full-scale prototype module has been constructed and its performance is currently being studied. As part of the construction phase of this chamber, details on the manufature of parts, feed-through deisgns, stringing of the chamber, structural supports and material choices have been addressed. In particular, aluminized kapton tubes were found superior to mylar tubes, and designs for plastic feed through systems have been completed. In addition, issues of gas handling have been resolved and a high voltage distribution board has been designed and built that seems to allow clean extraction of signals from the chamber.

Full cosmic ray studies are now underway with the goal of studying the resolution of the chamber as a function of crossing angle. In additon we need to determine if additional z information can be obtained by the use of charge division. While in the current tests, a preamplifier from the CLAS detector is being used, work is on-going with the electronics group at the University of Pennsylvania to develop an ASIC pre-amp design.

10. FDC

Forward drift chamber (FDC) prototypes have been built and are being tested using cosmic rays. Various techniques for constructing low-mass cathode planes are being tested. The University of Pennsylvania ASIC preamp design will also be used for the FDC system. Designed of a gas system are also underway. Beam tests in HALL B of a full-scale FDC module are planned for 2007.

TABLE III: Institutional responsibilities along with sources of support for the GlueX detector subsystems. Please see Figure 1 for the detector subsystem acronyms.

Institution	Responsibility	Support
Alberta	ELEC, BCAL	NSERC[a]
Athens		
Carnegie Mellon	CDC	DOE[b]
Catholic	BEAM	NSF[c]
Christopher Newport	TRIG	NSF
Connecticut	BEAM	NSF
Florida International	START	NSF
Florida State	UPV	DOE
Glasgow	TM	EPSRC[d]
Guanajuato		CONACyT[e]
IHEP (Protvino)	TM, TOF	MESRF[f]
Indiana	ELEC, TOF, FCAL, TRIG	DOE
Jefferson Lab	SCM, ELEC, DAQ	DOE
Ohio	FDC	NSF
Oak Ridge	PID	DOE
Regina	BCAL	NSERC
Tennessee	PID	DOE

[a]Natural Sciences and Engineering Research Council of Canada.
[b]Department of Energy - Office of Nuclear Physics.
[c]National Science Foundation.
[d]Engineering and Physical Sciences Research Council.
[e]Consejo Nacional de Ciencia y Tecnologia.
[f]Ministry for Education and Science of Russian Federation.

D. Institutional Responsibilities

The institutional responsibilities for the GlueX detector are summarized in Table III. Not included in this list are the theorists from various institutions who form the theory group within the GlueX collaboration. Software responsibilities are not listed explicitly but most of the collaborating institutions are involved in software for simulations and reconstruction.

E. Summary

The major GlueX detector subsystems are underway with institutions responsible for design, R & D and construction.

VI. GLUEX: THE FIRST TWO YEARS OF RUNNING

A. Overview

The GlueX run plan for the first two years is broken down into three phases. During Phase I (first six months) we will be doing low-level *detector commissioning* that requires neither 12 GeV electrons nor the ultimate emittance from the machine. During the detector commissioning phase the beam tagger will also be commissioned. During Phase II (following six months) we will systematically go through *physics commissioning* by studying well-known reactions, in particular, measuring the density matrix elements of diffractively produced ρ, ω and ϕ mesons to check out our event reconstruction and particle identification capabilities. During this phase we want to also study the photon beam linear polarization and measure how it tracks with electron beam emittance. It may be necessary during this phase to match the photon energy (adjust the crystal angle relative to the electron beam) to available electron energy to maximize polarization. Finally, in Phase III (the next twelve months) we will start *exploratory physics*, searching for exotic mesons in decay channels that are expected to be fertile channels for such searches and/or channels where tantalizing evidence for exotic meson signals have been reported. During this phase we plan on running with a 12 GeV electron beam at the design emittance of 10 mm·μr and at a flux of 10^7/s with some running at higher fluxes as we push toward the ultimate 10^8/s rate. The running conditions for the three phases are summarized in Table IV.

B. Event Rate & Yield Assumptions

The total event rate is given by equation 2, where the event rate is R, the total cross section is σ_T, the number of scattering centers per unit area in the target is N_t and the photon beam flux is N_γ.

$$R \;=\; \sigma_T \cdot N_t \cdot N_\gamma \tag{2}$$

The total hadronic cross-section, σ_T, for the reaction: $\gamma p \rightarrow$ anything at a photon energy of $E_\gamma = 9$ GeV is approximately 120 μb. The GlueX target is a 30 cm-long LH_2 cylinder and the number of scattering centers per area is

$$\begin{aligned} N_t \;&=\; 12.6 \times 10^{23}\ \mathrm{cm}^{-2} \text{ or} \\ &=\; 1.26\ \mathrm{b}^{-1}\,. \end{aligned}$$

A photon beam flux of $N_\gamma = 10^8$/s corresponds to an event rate R of 15 kHz. During initial running we will use a photon flux that is a factor of 10 smaller. Another way to express the event rate for a 30 cm-long LH_2 target is that with a photon beam flux of $N_\gamma = 10^7$/s, a 1 μb cross-section yields a rate of 12.5 Hz.

During Phases II and III we assume that the combined efficiency of accelerator, photon beam and GlueX detector will be 30% so for purposes of estimating yields Phases II and III, the effective integrated running time will be 2.5×10^6 s and 5×10^6 s respectively. Also, based on Monte Carlo studies, we estimate the combined geometric and reconstruction efficiencies for typical event topologies to be about 75%.

TABLE IV: GlueX Running Conditions - First Two Years

Quantity	Phase I[a]	Phase II[b]	Phase III[c]
Duration (months)	6	6	12
Min. electron energy (GeV)	10	11	12
Max. emittance (mm·μr)	50	20	10
Min. photon energy (GeV)	$8-9$	$8-9$	9
Photon Flux (γ/s)	10^6	10^7	10^7

[a]Detector commissioning
[b]Physics commissioning - appropriately match photon energy to electron energy to maximize polarization
[c]Exploratory physics at design energies and emittance. Some running will take place at a photon flux of 10^8/s.

C. Phase II Running

During Phase II running GlueX will collect data on well-measured reactions, such as the diffractive production of the vector mesons ρ, ω and ϕ, whose production cross-sections are listed in Table V. For a photon beam flux of $N_\gamma = 10^7$/s, including the overall detection efficiency, we expect to collect a total sample of 940M ρ events, 94M ω events and 18M ϕ events. The spin density matrix elements of these low-lying vector states have been determined in photoproduction with linearly polarized photons (*e.g.* see [89]). Various decay modes for these will be studied as well. For example the decays $\omega \to \pi^+\pi^-\pi^0$ and $\omega \to \pi^0\gamma$ occur with branching fractions of 89% and 9% respectively. And for the ϕ the decay modes into K^+K^-, 3π and $\eta\gamma$ occur with branching fractions of 49%, 15% and 1.3% respectively.

In addition to the vector states, the photoproduction of other mesons have also been measured – such as the $f_2(1270)$ and the $a_2(1320)$. Their production cross-sections are also listed in Table V. The decays of the $f_2(1270)$ into $\pi\pi$ and $K\bar{K}$ occur with branching fractions of 85% and 5% respectively. The $a_2(1320)$ decays into $\rho\pi$, $\eta\pi$, $\omega\pi\pi$, $K\bar{K}$ and $\eta'\pi$ with branching fractions of 70%, 15%, 10%, 5% and 0.5% respectively. It will be essential to focus on these decays and obtain consistent results within the amplitude analyses. These decay channels are also relevant for exotics searches.

Another physics topic of interest is the measurement of the spin structure of the K^+K^- system near threshold to study S-wave/P-wave interference – the S-wave states are the $a_0(980)$ and $f_0(980)$ while the P-wave state is the $\phi(1020)$ (see [90]).

D. Phase III Running

This exploratory physics Phase III of GlueX running will focus on the exotic nonets: 0^{+-}, 1^{-+} and 2^{+-} and in particular will focus on the decay channels $\rho\pi$, $b_1\pi$ and $a_2\pi$. As indicated in Table VI, these modes should access the $I = 0$ members of all three nonets and the $I = 1$ members of the 1^{-+} and 2^{+-} nonets.

TABLE V: Cross sections for various photoproduction reactions at a photon energy of 9 GeV.

Reaction	Approximate $\sigma(\mu$b)
$\gamma p \to \rho(770)p$	20
$\gamma p \to \omega p$	2
$\gamma p \to \phi p$	0.4
$\gamma p \to f_2(1270)p$	1
$\gamma p \to a_2^+(1320)n$	1
$\gamma p \to b_1^0(1235)p$	1
$\gamma p \to \rho'(1465)p$	1
$\gamma p \to (3\pi)^0 p$	10
$\gamma p \to (3\pi)^+ n$	10
$\gamma p \to (2\pi\omega)^0 p^a$	0.2
$\gamma p \to (2\pi\omega)^+ n$	0.2
$\gamma p \to (2\pi\eta)^0 p^b$	0.2
$\gamma p \to (2\pi\eta)^+ n$	0.2

[a]B.R.($\omega \to \pi^+\pi^-\pi^0$) = 89% and B.R.($\omega \to \pi^0\gamma$) = 9%
[b]B.R.($\eta \to \pi^+\pi^-\pi^0$) = 23% and B.R.($\eta \to 2\gamma$) = 39%

TABLE VI: Possible Decay Modes for Exotic Hybrids

Particle	J^{PC}	I	G	Possible Modes[a]
b_0	0^{+-}	1	+	
h_0	0^{+-}	0	−	$b_1\pi$
π_1	1^{-+}	1	−	$\rho\pi$, $b_1\pi$
η_1	1^{-+}	0	+	$a_2\pi$
b_2	2^{+-}	1	+	$a_2\pi$
h_2	2^{+-}	0	−	$\rho\pi$, $b_1\pi$

[a]Assuming the $G = +$ channel $2\pi\eta$ or the $G = -$ channels 3π or $2\pi\omega$.

The $\rho\pi$, $b_1\pi$ and $a_2\pi$ modes lead to the final states $3\pi N$, $2\pi\omega N$ and $2\pi\eta N$ respectively via the decay modes $\rho \to 2\pi$, $b_1 \to \omega\pi$ and $a_2 \to \eta\pi$. Table V lists the expected cross sections for these final states. We note that the 2π and $\omega\pi$ modes are dominant for the ρ and b_1 respectively and the branching fraction for $a_2 \to \eta\pi$ is 15%.

In understanding the entries of Table VI we remind the reader that the G-parity, isospin (I) and charge conjugation (C) are related as follows: $G = C\cdot(-1)^I$. For the 3π and $2\pi\omega$ channels $G = -$, and $G = +$ for $2\pi\eta$. For $\rho\pi$, $b_1\pi$ and $a_2\pi$ the isospin can be 0 or 1. The spins of these systems are given by given by the spin sums: $\vec{L}+\vec{1}$, $\vec{L}+\vec{1}$ and $\vec{L}+\vec{2}$ respectively (where L is the relative angular momentum between the two mesons) and the parities are given by $(-1)^L$, $(-1)^{L+1}$ and $(-1)^{L+2}$ respectively.

We note that photoproduction reactions resulting in the final states $3\pi N$, $2\pi\omega N$ and $2\pi\eta N$ will be particularly fruitful channels for exotics searches. The cross section estimates are listed in Table V.

The GlueX collaboration has extensive experience in analysis of the 3π system (see the earlier discussion on the analysis of the reactions $\pi^- p \to (3\pi)^- p$. The availability of multiple-decay modes for the ω and η will also be critical in understanding backgrounds and systematics.

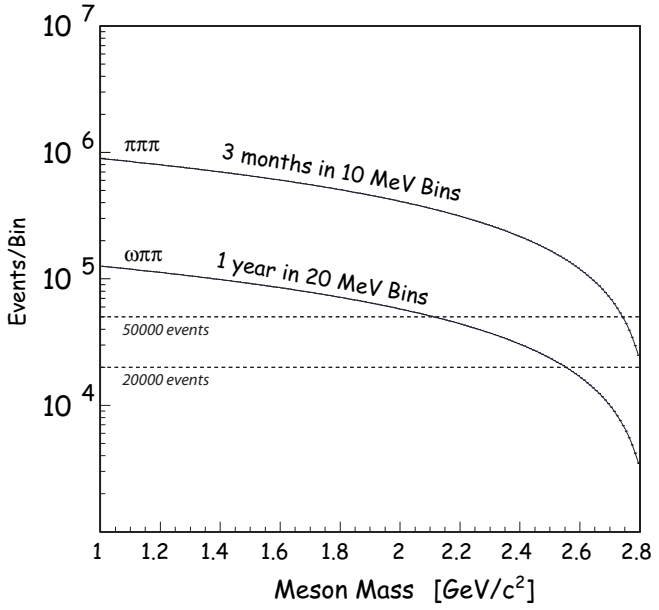

FIG. 18: Expected yields for the 3π channel per 10 MeV mass bin after 3 months of running as a function of mass, along with the expected yields for the $2\pi\omega$ channel per 20 MeV mass bin after 12 months of running as a function of mass. See the text for yield assumptions.

Figure 18 shows the expected yields for the 3π channel per 10 MeV mass bin after 3 months of running as a function of mass, along with the expected yields for the $2\pi\omega$ channel per 20 MeV mass bin after 12 months of running as a function of mass. The assumptions used for these estimates are:

1. There will be 26 weeks of 12 GeV operation with beam on the GlueX target. Of the 26 weeks, $\frac{1}{3}$ of it will produce useful data. This leads to 5×10^6 seconds of good beam per year.

2. Initially, the GlueX Detector will be able to handle a photon flux of 10^7 tagged photons per second on target.

3. The combination of solid angle and reconstruction efficiency will allow us to use approximately 75% of the events that are collected to tape.

The expected yields of data on the $3\pi N$ and $2\pi\omega N$ final states will exceed the E852 data by at least 2-3 orders of magnitude. The expected yields for the $2\pi\eta N$ final state will require longer running to achieve the same level of sensitivity.

E. Summary

The run plan for the first two years of GlueX operation will include full commissioning of the detector and beam tagging system, an understanding of how the photon beam polarization tracks with beam emittance, correlating beam polarization information with the spin density matrices of diffractively produced vector mesons, a detailed amplitude analysis of well-known states, such as the $a_2(1320) \rightarrow 3\pi$, preliminary information on excited vector mesons and finally an exploratory look at the amplitude analysis of channels that could yield information on exotic hybrid states. The second year of data taking will require 12 GeV electrons at the required emittance.

[1] G. S. Bali et al., Phys. Rev. D **62**, 054503 (2000), [SESAM/TCL Collaboration].
[2] Y. Nambu, Tech. Rep., U. of Chicago Report No. 70-70 (1970).
[3] N. Isgur and J. Paton, Phys. Rev. **D31**, 2910 (1985).
[4] C. Bernard et al., Phys. Rev. **D56**, 7093 (1997), [MILC Collaboration].
[5] T. D. Cohen, Phys. Lett. B **427**, 348 (1998), arXiv: hep-ph/9801316.
[6] *A resource for the international lattice gauge theory community*, URL `http://www.lqcd.org`.
[7] A. Afanasev and P. R. Page, Phys. Rev. A **57**, 6771 (1998).
[8] A. P. Szczepaniak and M. Swat, Phys. Lett. B **516**, 72 (2001).
[9] D. Aston et al., Tech. Rep., SLAC (1986), sLAC-REP-298.
[10] F. J. Barbosa et al., Nuclear Science Symposium Conference Record 2002 IEEE p. 135 (2002).
[11] B. S. Zhou and D. V. Bugg, Eur. Phys. J. **16**, 537 (2003).
[12] S. U. Chung, Tech. Rep. (2004), bNLQGS-02-0900.
[13] A. Anisovich et al., Eur. Phys. J. **24**, 111 (2005).
[14] A. Anisovich et al., Eur. Phys. J. **25**, 427 (2005).
[15] A. Anisovich et al., Eur. Phys. J. **25**, 441 (2005).
[16] C. Aubin et al., Phys. Rev. **D70**, 094505 (2004), hep-lat/0402030.
[17] T. Burch et al., Phys. Rev. **D73**, 094505 (2006), hep-lat/0601026.
[18] S. Basak et al., Nucl. Phys. Proc. Suppl. **153**, 242 (2006), hep-lat/0601034.
[19] P. Lacock, C. Michael, P. Boyle, and P. Rowland (UKQCD), Phys. Lett. **B401**, 308 (1997), hep-lat/9611011.
[20] P. Lacock, C. Michael, P. Boyle, and P. Rowland (UKQCD), Phys. Rev. **D54**, 6997 (1996), hep-lat/9605025.
[21] C. W. Bernard et al., Nucl. Phys. Proc. Suppl. **53**, 228 (1997), hep-lat/9607031.
[22] C. W. Bernard et al. (MILC), Phys. Rev. **D56**, 7039 (1997), hep-lat/9707008.
[23] P. Lacock and K. Schilling (TXL), Nucl. Phys. Proc. Suppl. **73**, 261 (1999), hep-lat/9809022.

[24] C. McNeile et al., Nucl. Phys. Proc. Suppl. **73**, 264 (1999), hep-lat/9809087.
[25] C. Bernard et al., Phys. Rev. **D68**, 074505 (2003), hep-lat/0301024.
[26] J. N. Hedditch et al., Phys. Rev. **D72**, 114507 (2005), hep-lat/0509106.
[27] C. McNeile and C. Michael (UKQCD), Phys. Rev. **D73**, 074506 (2006), hep-lat/0603007.
[28] A. W. Thomas and A. P. Szczepaniak, Phys. Lett. **B526**, 72 (2002), hep-ph/0106080.
[29] M. Luscher, Nucl. Phys. **B364**, 237 (1991).
[30] J. J. Dudek, R. G. Edwards, and D. G. Richards, Phys. Rev. **D73**, 074507 (2006), hep-ph/0601137.
[31] M. S. Cook and H. R. Fiebig (2006), hep-lat/0606005.
[32] T. Burns and F. E. Close (2006), hep-ph/0604161.
[33] N. Isgur, Phys. Rev. **D60**, 114016 (1999), hep-ph/9904494.
[34] F. E. Close and J. J. Dudek, Phys. Rev. **D69**, 034010 (2004), hep-ph/0308098.
[35] F. E. Close and J. J. Dudek, Phys. Rev. Lett. **91**, 142001 (2003), hep-ph/0304243.
[36] N. Isgur, R. Kokoski, and J. E. Paton, Phys. Rev. Lett. **54**, 869 (1985).
[37] F. E. Close and P. R. Page, Nucl. Phys. **B443**, 233 (1995), hep-ph/9411301.
[38] P. R. Page, E. S. Swanson, and A. P. Szczepaniak, Phys. Rev. **D59**, 034016 (1999), hep-ph/9808346.
[39] R. Kokoski and N. Isgur, Phys. Rev. **D35**, 907 (1987).
[40] P. R. Page, Phys. Lett. **B402**, 183 (1997), hep-ph/9611375.
[41] F. Iddir, A. Le Yaouanc, L. Oliver, O. Pene, and J. C. Raynal, Phys. Lett. **B207**, 325 (1988).
[42] T. H. Bauer et al., Rev. Mod. Phys. **50**, 261 (1978).
[43] S. Godfrey and J. Napolitano, Rev. Mod. Phys. **71**, 1411 (1999).
[44] E. Klempt, Tech. Rep. (2004), arXiv: hep-ph/0404270.
[45] D. Alde et al., Phys. Lett. B **205**, 397 (1988).
[46] S. F. Tuan, T. Ferbel, and R. H. Dalitz, Phys. Lett. B **213**, 537 (1988).
[47] Y. Prokoshkin and S. Sadovsky, Phys. Atom. Nucl. **58**, 853 (1995).
[48] Y. Prokoshkin and S. Sadovsky, Phys. Atom. Nucl. **58**, 606 (1995).
[49] G. M. Beladidze et al., Phys. Lett. B **313**, 276 (1993).
[50] H. Aoyagi et al., Phys. Lett. B **314**, 246 (1993).
[51] D. R. Thompson et al., Phys. Rev. Lett. **79**, 1630 (1997), (E852 Collaboration).
[52] S. U. Chung et al., Phys. Rev. D **60**, 092001 (1999), (E852 Collaboration).
[53] A. Abele et al., Phys. Lett. B **423**, 175 (1998), (Crystal Barrel Collaboration).
[54] A. Abele et al., Phys. Lett. B **446**, 349 (1999), (Crystal Barrel Collaboration).
[55] A. R. Dzierba et al., Phys. Rev. D **67**, 094015 (2003), (Subset of the E852 Collaboration).
[56] J. Gunter et al., Phys. Rev. D **64**, 072003 (2001), (E852 Collaboration).
[57] A. P. Szczepaniak, M. Swat, A. Dzierba, and S. Teige, Phys. Rev. Lett. **91**, 092002 (2003).
[58] E. I. Ivanov et al., **86**, 3977 (2001), (E852 Collaboration).
[59] J. Reinnarth et al., Nucl. Phys. A **692**, 268c (2001), (Crystal Barrel Collaboration).
[60] G. S. Adams et al., Phys. Rev. Lett. **81**, 5760 (1998), (E852 Collaboration).
[61] S. U. Chung et al., Phys. Rev. D **65**, 072001 (2002), (E852 Collaboration).
[62] D. V. Amelin et al., Phys. Atom. Nucl. **68**, 359 (2005), (VES Collaboration).
[63] A. R. Dzierba et al., Phys. Rev. D **73**, 072001 (2006), (Subset of the E852 Collaboration).
[64] J. Kuhn et al., Phys. Lett. B **595**, 109 (2004), (E852 Collaboration).
[65] M. Lu et al., Phys. Rev. Lett. **94**, 032002 (2005), (E852 Collaboration).
[66] F. E. Close, A. Donnachie, and Y. S. Kalashnikova, Phys. Rev. D **65**, 092003 (2002).
[67] S. Eidelman et al., Phys. Lett. B **592**, 1 (2004).
[68] S. Eidelman et al., Phys. Lett. B **592**, 576 (2004).
[69] R. Mitchell, U. of Tennessee Dept. of Physics Ph. D. Thesis.
[70] A. Donnachie (2001), hep-ph/0106197.
[71] A. Donnachie and Y. S. Kalashnikova (2001), hep-ph/0110191.
[72] A. Donnachie (1991), Invited talk at Hadron '91 - U. of Mayland.
[73] A. Donnachie and A. B. Clegg, Nucl. Phys. B (Proc. Suppl.) **21**, 118 (1991).
[74] P. Lacock and K. Schilling, Nucl. Phys. Proc. Suppl. **73**, 261 (1999), hep-lat/9809022.
[75] J. Ballam et al., Phys. Rev. D **7**, 3150 (1973).
[76] F. Cooper, Phys. Rev. **170** (1968).
[77] R. Thews, Phys. Rev. **175**, 1749 (1968).
[78] K. Schilling, P. Seyboth, and G. Wolf, Nucl. Phys. B **15**, 397 (1970).
[79] A. Afanasev and A. Szczepaniak, Rhys. Rev. D **61**, 114008 (2000).
[80] MCFast, Tech. Rep., Fermilab (2000), URL `http://cepa.fnal.gov/psm/simulation/mcfast/`.
[81] R. Mankel, Rep. Prog. Phys. **67**, 553 (2004).
[82] R. Frühwirth, M. Regler, R. Bock, H. Grote, and D. Notz, *Data Analysis Techniques for High Energy Physics, second edition* (Cambridge Press, 2000), chapter 2.
[83] B. Brabson et al., Nuclear Inst. and Meth. A **332**, 419 (1993).
[84] R. R. Crittenden et al., Nucl. Instrum. Meth. A **387**, 377 (1997).
[85] R. J. *et al.*, submitted to Nucl. Instrum. Meth. (2004).
[86] S. Denisov et al., Nucl. Instrum. Meth. A **478**, 440 (2002).
[87] S. Denisov et al., Nucl. Instrum. Meth. A **525**, 183 (2004).
[88] S. Denisov et al., Nucl. Instrum. Meth. A **494**, 495 (2002).
[89] J. Ballam et al., Phys. Rev. Lett. **24**, 960 (1970).
[90] D. C. Fries et al., Nucl. Phys. B **143**, 408 (1978).
[91] The "f_1" here is just the connected part of the amplitude and as such is forced to be degenerate with the a_1
[92] and indeed it is possible within the flux-tube model to have such partial widths large if the pion is treated asymmetrically from the rho